The Development of the 3D Micropatterned ECM (Extracellular Matrix) Models of Glioma-Astrocyte Co-culture: Investigating Glioma Migration and Astrocyte Reactivity

by

Nilufar Ismayilzada

A Dissertation Submitted to the

Graduate School of Sciences and Engineering

in Partial Fulfillment of the Requirements for

the Degree of

Master of Science

in

Biomedical Sciences and Engineering

KOÇ
ÜNİVERSİTESİ

January 26, 2024

The Development of the 3D Micropatterned ECM (Extracellular Matrix) Models of Glioma-Astrocyte Co-culture: Investigating Glioma Migration and Astrocyte Reactivity

Koç University

Graduate School of Sciences and Engineering

This is to certify that I have examined this copy of a master's thesis by

Nilufar Ismayilzada

and have found that it is complete and satisfactory in all respects,

and that any and all revisions required by the final

examining committee have been made.

Committee Members:

Assist. Prof. Emel Sokullu (Advisor)

Prof. Dr. Engin Ulukaya

Assist. Prof. Zelal Adıgüzel

Date: 26.01.24

ABSTRACT

The Development of the 3D Micropatterned ECM (Extracellular Matrix) Models of Glioma-Astrocyte Co-culture: Investigating Glioma Migration and Astrocyte Reactivity

Nilufar Ismayilzada

Master of Science in Biomedical Sciences and Engineering

January 26, 2024

Glioblastoma multiforme (GBM) is the most fatal type of primary malignant brain tumors, characterized by aggressive infiltration into brain tissue. GBM migration is a complex process affected by several factors, including the bilateral communication between the GBM tumor and its microenvironment (TME). Astrocytes, the star-shaped stromal components of the GBM TME, account for half of the brain cells; however, their exact role within GBM invasiveness remains not fully understood. The utilization of scaffold-based 3D cell culture platforms has emerged as a promising strategy to mimic the complexity of the GBM TME. Among them, hydrogels with tunable biochemical and mechanical properties are ideal for replicating the low-stiffness and well-hydrated extracellular matrix (ECM) of the brain. The photocrosslinkable, semi-synthetic hydrogel, gelatin methacrylate (GelMA) offers advantages of cell-responsiveness and biodegradability, simultaneously providing a fine level of control over its mechanical properties, including matrix stiffness and porosity. In this thesis, it was aimed to establish an in vitro 3D co-culture model of the GBM TME. To accomplish this goal, a two-step photolithography technique with photomasks was employed to surround high-stiffness U87 GBM cells encapsulated in GelMA microspheres, resembling glioma tumors, by lower-stiffness GelMA matrices, mimicking the healthy brain parenchyma. This technique facilitated the establishment of two distinct astrocyte-glioma co-culture configurations, demonstrating the versatility of the proposed microfabrication technique in precisely localizing various cell types. The quantitative analysis of time-lapse confocal microscopy images revealed the differential impact of the immortalized normal human astrocyte (I-NHA) co-culture configuration on GBM migration. Encapsulating I-NHA cells in vicinity to U87 GBM cells resulted in extensive invasion of the surrounding GelMA matrix by GBM cells. In contrast, surrounding U87 GBM microspheres with an astrocyte-dispersed matrix led to the establishment of the astrocytic network, which inhibited the tumor cell migration. To further validate the physiological relevance of the microfabricated platform, we performed the immunofluorescent staining and qPCR analysis of proteins and genes related to GBM migration and malignancy as well as astrocyte reactivity. The immunocytochemical staining confirmed the upregulation of GFAP expression by interconnected astrocytic networks around U87 microspheres, suggesting the reactive transformation of astrocytes and the formation of the glial scar in the presence of GBM cells. Additionally, culturing U87 cells in the 3D environment of GelMA microspheres resulted in the upregulation of genes linked to GBM invasiveness, including MMP family proteases (MMP-2, MMP-9, MMP-14), hypoxia-related factors (VEGF, HIF-1α), and epithelial-to-mesenchymal transition (EMT) markers (CD44, FN1, TGF-β). In conclusion, this thesis presents a 3D micropatterned co-culture model of the GBM TME, offering a novel biomimetic in vitro tool for advancing our understanding of GBM migration and the intricate dynamics within the GBM TME.

ÖZETÇE

Glioma-Astrosit Ko-kültürünün 3B Mikrodesenli ECM (Ekstraselülar Matriks) Modellerinin Geliştirilmesi: Glioma Migrasyonu ve Astrosit Reaktivitesinin İncelenmesi

Nilüfer İsmayilzada

Biyomedikal Bilimler ve Mühendisliği, Yüksek Lisans

26 Ocak 20

Glioblastoma multiforme (GBM) beyin dokusuna agresif infiltrasyon ile karakterize, primer malign beyin tümörlerinin en ölümcül tipidir. GBM migrasyonu, glioblastoma ile tümör mikroçevresi (TMÇ) arasında karşılıklı iletişimi de içeren birçok faktörden etkilenen kompleks bir süreçtir. GBM TMÇ'nin stromal komponenti olan yıldız şekilli astrositler, beyin hücrelerinin yarısını oluşturur, ancak GBM invazyonundaki kesin rolü tam olarak anlaşılamamıştır. İskele-tabanlı 3 boyutlu (3B) hücre kültürü platformlarının kullanılması GBM TMÇ'nin kompleksliğini taklit etmek için umut verici bir strateji olarak ortaya çıkmıştır. Fotoçaprazlanabilir bir semi-sentetik hidrojel olan gelatin methacrylate (GelMA) hücre duyarlılığı ve biyolojik parçalanabilirlik avantajları sunarken, aynı zamanda matris sertliği ve porozite dahil olmak üzere mekanik özellikleri üzerinde iyi düzeyde kontrol sağlar. Bu tezde, GBM TMÇ'nin in vitro 3B ko-kültür modelinin oluşturulması amaçlanmıştır. Bu hedefe ulaşmak için, yüksek sertlikteki GelMA mikrosferleri içinde kapsüllenmiş U87 GBM hücrelerini, sağlıklı beyin parankimini taklit eden daha düşük sertlikteki GelMA matrisleri ile çevrelemek için fotomasklı iki aşamalı fotolitografi tekniği kullanılmıştır. Bu teknik, iki farklı astrosit-glioma ko-kültür konfigürasyonunun oluşturulmasını kolaylaştırdı ve önerilen mikrofabrikasyon tekniğinin çeşitli hücre tiplerini tam olarak lokalize etmedeki çok yönlülüğünü ortaya koydu. Time-lapse konfokal mikroskop görüntülerinin kantitatif analizi, ölümsüzleştirilmiş normal insan astrosit (I-NHA) ko-kültür konfigürasyonunun GBM migrasyonu üzerindeki farklı etkisini ortaya çıkardı. I-NHA hücrelerinin U87 GBM hücrelerinin yakınında kapsüllenmesi, çevredeki GelMA matrisinin geniş çapta istilasına neden oldu. Buna karşılık U87 GBM mikrosferlerinin astrosit dağılmış bir matris ile çevrelenmesi, tümör hücrelerinin göçünü engelleyen bir astrocytik ağın oluşmasına neden oldu. Platformun fizyolojik uygunluğunu daha da doğrulamak için, GBM migrasyonu ve astrosit reaktivitesi ile ilgili genlerin ve proteinlerin immünofloresan ve qPCR analizini gerçekleştirdik. İmmünositokimyasal boyama, U87 hücrelerinin varlığında birbirine bağlı astrositik ağlar tarafından GFAP ekspresyonunun upregülasyonunu doğrulamakta, astrositlerin reaktif transformasyonunu ve U87 GBM mikrosferleri çevresinde glial skar oluşumunu düşündürmektedir. Ek olarak, U87 hücrelerinin 3D GelMA mikrosfer ortamında kültürlenmesi, MMP ailesi proteazları (MMP-2, MMP-9, MMP-14), hipoksi ile ilişkili faktörler (VEGF, HIF-1α) ve epitel mezenkimal transition (EMT) belirteçleri (CD44, FN1, TGF-β) dahil olmak üzere GBM invazivliği ile bağlantılı genlerin upregülasyonuyla sonuçlandı. Sonuç olarak bu tez, GBM TMÇ'nin 3 boyutlu mikropaternli ko-kültür modelini, GBM TMÇ içindeki karmaşık dinamikleri ve GBM migrasyonunu anlamamızı geliştirmek için yeni bir biyomimetik in vitro araç sunmaktadır.

ACKNOWLEDGEMENTS

I would like to thank the following people without whom I would not have made it through my Master's degree! I would like to express my sincere gratitude to my supervisor Professor Emel Sokullu who provided me with consistent support through this journey. Her encouragement and belief in my potential have not only motivated me but also shaped the trajectory of my research. I would like to thank my colleague, Ecem Metin, her mentorship in the laboratory was crucial in improving my research skills. Her companionship and support made the often solitary journey of research a collaborative and enjoyable experience. A debt of gratitude is also owed to Ismayil Can Karaoglu and Banu Erdem for helping with rheological measurements and image processing. I am also thankful to Haroon Qureshi for performing the fluorescent tagging of my cells.

I am immensely grateful to my roommate, Maryam Kahvazizadeh. Her presence was a beacon of support and comfort during my most challenging times. Her ability to listen, encourage, and stand by me was a constant source of strength. I would also like to thank my roommates Eda and Beste for their vibrant and positive energy. I will not forget our late-night conversations about the meaning of life, philosophy and much more. Special thanks to beautiful Nurbahar, for being a source of inspiration with her strength and grace. Most importantly, I would like to thank my family always being there for me. Their endless support, love, and belief in me have been the foundation of my success. Their presence in my life has been the most significant source of encouragement and strength.

TABLE OF CONTENTS

LIST OF TABLES ..... **VIII**

LIST OF FIGURES ..... **IX**

ABBREVIATIONS ..... **XI**

CHAPTER 1: INTRODUCTION **1**

CHAPTER 2: LITERATURE REVIEW **2**

2.1 Glioblastoma Multiforme (GBM): General Introduction 2

2.2 The Dynamics of Glioma Cell Migration and Invasion in the Brain 3

2.3 The Role of Tumor Microenvironment in GBM 6

2.4 Astrocytes in Healthy Brain and in GBM 7

2.5 In-vitro Co-culture Studies Investigating the role of Astrocytes in GBM Invasiveness and Migration 9

2.6 GelMA hydrogel as a 3D Culture System for Modelling GBM Microenvironment 11

CHAPTER 3: MATERIALS AND METHODS **14**

3.1 Cell Culture 14

3.2 Coating of Glass Slides 14

3.3 GelMA Synthesis 14

3.4 Scanning Electron Microscopy (SEM) 15

3.5 Rheology Measurements of GelMA Storage Modulus 15

3.6 GelMA Prepolymer Solution Preparation 16

3.8 Cell Viability Assays 18

3.9 Phalloidin Staining of U87 Cytoskeletal Organization 18

3.10 RNA Extraction from Hydrogel Constructs 19

3.11 Gene Expression Analysis by Real Time Quantitative PCR (RT-qPCR) 19

3.12 GFP and RFP tagging of U87 and I-NHA Cells Lines 21

3.13 Co-culture Experimental Setups for Gene and Protein Expression Analysis 21

3.13.1 Co-culture Experimental Setup for qPCR analysis of Gene Expression 21

3.13.2 Co-culture Setup for Immunofluorescent Staining against GFAP 21

3.14 Image Processing for Migration Analysis 22

CHAPTER 4: RESULTS AND DISCUSSION 23

4.1 Characterization of GelMA Mechanical Properties..... 23

4.2 Viabilities of U87 GBM and I-NHA Cell Lines inside GelMA Constructs…….25

4.2.1 Quantitative Assessment of the Cell Concentration Impact on Cell Viability……...25

4.2.2 Qualitative Evaluation of the Culture Duration on Cell Viability via Live/Dead Assay..... 28

4.3 Development of the Micropatterned Tumor Model..... 30

4.4 Visualization of Cytoskeletal Organization of U87 GBM Cells within the Micropatterned Tumor Model 31

4.5 Establishment of 3D Micropatterned Co-culture Models of Glioma-Astrocyte Interactions 36

4.6 The Impact of U87 Cells on Astrocyte Reactivity..... 44

4.7 Gene Expression Analysis of U87 Cells inside the Micropatterned Model of the GBM TME..... 47

4.7.1 Gene Expression Analysis of the 3D Culture Effect on U87 GBM Cells……. 48

4.7.2 Gene Expression Analysis of the I-NHA Co-culture Effect on the Co-culture System..... 52

4.7.3 Evaluation of the Co-culture Configuration Effect on the Gene Expression of the Co-culture System..... 53

CHAPTER 5: CONCLUSIONS AND FUTURE PERSPECTIVES..... 56

BIBLIOGRAPHY..... 59

LIST OF TABLES

Table 1: List of Primers Used for qPCR

LIST OF FIGURES

Figure 4.1. Characterization of GelMA mechanical properties……23

Figure 4.2 The impact of cell concentration and culture duration on the viability of I-NHA and U87 cells within GelMa constructs assessed via MTT assay..... 25

Figure 4.3 The impact of culture duration on the viability of I-NHA and U87 cells within GelMa constructs assessed via Live/Dead assay..... 28

Figure 4.4 The effect of culture duration on U87 cell behavior inside the micropatterned tumor model 30

Figure 4.5 Morphological assessment of U87 within the micropatterned tumor model via phalloidin staining……31

Figure 4.6 Morphological assessment of U87 within the micropatterned tumor model via α-tubulin staining..... 33

Figure 4.7 Cytoskeletal organization of cells embedded within GelMA circular constructs of varying stiffness values..... 35

Figure 4.8 Comparative dynamics of two U87-NHA 3D co-culture configurations with 2mil/ml I-NHA and 1mil/ml U87 cell densities...... 36

Figure 4.9 Comparative dynamics of two U87-NHA 3D co-culture configurations with 2mil/ml I-NHA and 3 mil/ml U87 cell densities...... 39

Figure 4.10 3D projections of representative images of two co-culture configurations at Day 7 of culture 40

Figure 4.11 Quantitative assessment of the co-culture configuration type on U87 GBM cell line migration capacity. 42

Figure 4.12 Astrocytic network development around U87 tumor microspheres...... 44

Figure 4.13 The immunocytochemical analysis of astrocyte reactivity around U87 microspheres..... 45

Figure 4.14 The bar charts visually representing the gene expressions of invasion-related MMP enzymes and hypoxia-related factors (VEGF and HIF-1α) as determined by quantitative real-time PCR. 48

Figure 4.15 The bar charts visually representing the expression profiles of genes related to epithelial-to-mesenchymal transition (EMT) in U87 cell line as determined by quantitative real-time PCR. 48

Figure 4.16 The bar charts depict the effect of I-NHA co-culture on the gene expression level of the co-culture system……..52

Figure 4.17 The bar charts depict the effect of co-culture configuration type on the gene expression level of the co-culture system……53

ABBREVIATIONS

TMZ	Temozolomide
GBM	Glioblastoma Multiforme
TME	Tumor microenvironment
ECM	Extracellular matrix
IDH	Isocitrate dehydrogenase
BBB	Blood-brain barrier
EGFR	Epidermal growth factor receptor
PDGFRA	Platelet-derived growth factor receptor alpha
FGF	Fibroblast growth factor
EMT	Epithelial-Mesenchymal transition
MMPs	Matrix Metalloproteinases
uPA	Urokinase-type plasminogen activator
HA	Hyaluronic acid
GAGs	Glycosaminoglycans
GLAST	Glutamate aspartate transporters
CNS	Central nervous system
GFAP	Glial fibrillary acidic protein
BDNF	Brain derived neurotrophic factor
CCL2	C-C motif chemokine ligand 2
IL-6	Interleukin 6
TAAs	Tumor-associated astrocytes
VEGF	Vascular endothelial growth factor
HAS2	Hyaluronan synthase 2
GelMA	Gelatin methacrylate
TMSPMA	3-(trimethoxysilyl)propyl methacrylate
MA	Methacrylic anhydride
FE-SEM	Field Emission Scanning Electron Microscope

EHT	Electron high tension
DMSO	dimethyl sulfoxide
MTT	(3-(4,5-Dimethylthiazol-2-yl)-2,5-Diphenyltetrazolium Bromide)
DMEM	Dulbecco's Modified Eagle Medium
FBS	Fetal bovine serum
PFA	Paraformaldehyde
BSA	Bovine serum albumin
DPBS	Dulbecco's phosphate-buffered saline
PI	Photoinitiator
CSPG	Chondroitin sulfate proteoglycans
MAO-B	Monoamine oxidase B
FACs	Fluorescence-activated cell sorting
HIF-1α	Hypoxia inducible factor
TGF-β	Tumor growth factor

Chapter 1:

INTRODUCTION

GBM is the most lethal type of primary brain tumors, comprising 50% of brain tumor incidences in adults (Shieh et al., 2020). Despite the administration of Stupp protocol, involving surgical resection with simultaneous radiotherapy and chemotherapy treatment with TMZ, GBM recurs or evolves resistance to traditional treatment modalities (Wu et al., 2021). Therefore, the prognosis for GBM remains dismal, with only 15-month of median survival rate (Davis, 2016). One of the main reasons of GBM malignancy and recurrence is its infiltrative pattern of invasion, which allows GBM cells to escape the complete surgical removal by migrating far into the healthy brain parenchyma (Seker-Polat et al., 2022). Understanding the precise mechanisms underlying the invasion of glioma cells is of great significance for the development of novel therapeutic strategies for GBM treatment.

There have been several in vitro methods developed to elucidate the GBM migration (Chen et al., 2022; Hashimoto et al., 2023). These techniques include the monolayer wound healing assay, which tracks cell movement in a scratched monolayer; the microliter-scale migration assay, assessing cell migration on ECM-coated slides; the Transwell migration assay, where cells migrate through a porous membrane towards an attractant; and the brain slice invasion assay, observing cell movement on rat brain slices (Bouchalova & Bouchal, 2022). Nevertheless, all these methods examine the migration of GBM in 2D, which is not representative of the 3D microenvironment of the GBM. GBM tumors exist within a complex tumor microenvironment (TME), comprising ECM and various cellular constituents, including astrocytes, microglia, and endothelial cells (Sharma et al., 2023). These elements play a pivotal role in facilitating GBM's invasiveness. Therefore, there is a current need for an in vitro 3D biomimetic model that recapitulates the intricate nature of the GBM TME, thereby providing a more accurate framework for studying GBM migration.

This thesis aimed to develop and validate a 3D micropatterned co-culture model of the GBM TME for GBM migration studies. The 3D model was fabricated by using a two-step lithography technique with photocrosslinkable hydrogel, GelMA and

photomasks. This novel technique enabled a precise control over cell localization and GelMA mechanical properties such as stiffness and porosity. The following chapters will further elaborate on the background of GBM and its migration (Chapter 2), the methodology for the co-culture model development and investigation (Chapter 3), and a detailed discussion of the main findings of this study (Chapter 4). Finally, Chapter 5 provides a conclusion and describes potential directions for future research utilizing the proposed micropatterned GBM TME model.

Chapter 2:

LITERATURE REVIEW

2.1 Glioblastoma Multiforme: General Introduction

Glioblastoma multiforme is the most prevalent and fatal primary malignant brain tumor. The average survival rate of patients diagnosed with GBM is around 15 months, whereas a 5-year survival rate accounts for only 6.8% (Weller et al., 2015). The aggressiveness and treatment-resistance of GBM stems from its complex inter- and intra- tumor heterogeneity, angiogenesis and diffuse infiltrative pattern of invasion into the surrounding brain tissue (Rabah et al., 2023).

Gliomas, due to their significant variability both among different patients and within individual tumors, are categorized through various criteria. One common approach to categorize these tumors involves the examination of specific genetic alterations. These alterations encompass mutations such as those found in IDH, gene amplifications affecting receptors like EGFR and PDGFRA, or modifications in gene regulation, such as promoter methylation in the MGMT gene (Bikfalvi et al., 2023). Additionally, transcriptomic profiling of the tumor bulk tissue has facilitated the classification of GBM cells into three distinct molecular states: mesenchymal, proneural, and classical (Chen et al., 2017). Possessing an increased aggressiveness

and angiogenesis capacity, cells of mesenchymal subtype are associated with chemoresistance and a poorer prognosis in patients. They display an elevated expression of astrocytic and mesenchymal markers corresponding to transdifferentiated and dedifferentiated tumors (Azam et al., 2020). Proneural class is associated with point mutations in IDH1 and alterations in PDGFRA. Tumors of this state are less aggressive compared to other classes and have a better prognosis (Verhaak et al., 2010). The classical subtype is distinguished by amplification of the EGFR as well as neural precursor and stem cell marker overexpression (Verhaak et al., 2010).

Furthermore, GBM tumors possess distinct histological regions including necrotic core, pseudopalisade or infiltrating rim, and tumor periphery (Brat et al., 2004; Wolf et al., 2019). Due to the rapid growth of glioma cells, their oxygen demand usually exceeds the available oxygen supply, resulting in the formation of hypoxic cores in the center of GBM tumors. The formation of ischemic regions within the tumor core results in the metabolic shift and migration of rapidly proliferating cells to tumor edges, where they establish regions of high cellular density, or pseudopalisades (Krawczynski et al., 2020) . Pseudopalisades are a distinct histopathological feature of malignant GBM tumors, which are formed by cells aligned in radial pattern around the tumor center. These zones are marked by high matrix production and cellular migration into the tumor periphery (Brat et al., 2004).

2.2 The Dynamics of Glioma Cell Migration and Invasion in the Brain

In contrast to other malignant tumors, which intravasate the lymphatic and circulatory systems, GBM rarely metastasizes beyond the confines of the brain. Instead, GBM tumor cells extensively infiltrate the surrounding healthy brain parenchyma far away from the tumor margin. Glioma cells migrate predominantly along axonal tracts, blood vessels and the subarachnoid space (Seker-Polat et al., 2022). Tumor cells invading the healthy brain parenchyma digest and remodel the surface of myelinated tracts. Furthermore, tumor cells migrate very fast along vasculature which provides

them with nutrients (Mair et al., 2018). Both white matter tracts and blood vessels offer a linear migratory pathway to glioma cells, potentially facilitating their distant migration (Gupta et al., 2024).

The tumor cell migration broadly takes place in four main steps: detachment from the primary tumor, breakdown of the ECM components, establishment of new connections with ECM, followed by the reorganization and contraction of the cell cytoskeleton (Fife et al., 2014). Cells initiate migration in response to diverse migratory signals, including but not limited to mechanical, chemical and electrical cues (Mair et al., 2018). As an example, glioma cells perceive haptotactic and vascular-derived chemotactic cues originating from the vascular basement membrane and interconnected axon tracts, propelling their collective migration (Wolf et al., 2019). Notably, glioma cells have a propensity to overexpress genes encoding chemokine and growth factor receptors, including those for EGF, FGF, and PDGF. This overexpression renders them more responsive and sensitive to chemotactic signals present in their environment (Mair et al., 2018).

The detachment of migratory cells from the tumor bulk requires the reduction of connections promoting cell-to-cell adhesion (Vollmann-Zwerenz et al., 2020). Migrating neoplastic cells of epithelial origin undergo a reversible cellular reprogramming, transitioning from an adhesive and polarized state to a fibroblast spindle-like phenotype, thereby acquiring the ability to migrate in a process, known as EMT epithelial-mesenchymal transition (Oishi et al., 2022). Despite glioma cells being of pro-neural origin, a transdifferentiation process akin to EMT occurs in these cells. This plasticity is triggered by specific ligand binding, leading to the activation of transcription factors, including Snail (Snail1), Slug (Snail2), ZEB1/2, and Twist1/2 (Vollmann-Zwerenz et al., 2020). As an example, TGF-β is an important player in inducing EMT in GBM through the activation of downstream signalling pathways, including PI3K, SMADs and MAPK (Oishi et al., 2022). TGF-β was shown to activate a mesenchymal phenotype in GBM via expression of SMAD2 and ZEB1 transcription factors (Joseph et al., 2014). EMT-related transcription factors, in turn, promote the expression of genes typically associated with mesenchymal cells, such as N-cadherin (CDH2), vimentin, and fibronectin (Debnath et al., 2022).

In order to facilitate the migratory process, GBM cells remodel and degrade the ECM. The ECM degradation is promoted through the secretion of MMPs. MMPs

comprise a large family of endopeptidases, including the secreted gelatinases MMP-2 and MMP-9 (Ciasca et al., 2016). This particular subset of MMPs is characterized by its ability to cleave type IV collagen, thereby contributing to the migration of malignant glioma cells through digestion of the brain's ECM (Quintero-Fabián et al., 2019). The activation of MMPs is usually mediated by serine proteases (e.g. plasmin, uPA) and other MMPs(e.g., MMP-14) (Sternlicht & Werb, 2001). Alternatively, migrating GBM cells can mechanically deform the ECM by exerting tensile and compressive forces (Beeghly et al., 2022).

Despite glioma cells degrading the brain ECM through the release of proteases, navigating through the brain parenchyma remains a formidable challenge. The healthy brain tissue is characterized by tightly packed cellular processes with submicron pore sizes (Mair et al., 2018). Following the perception of migratory signals, glioma cells undergo polarization, establishing a leading edge in the direction of migration and a trailing edge at the rear (Zhong et al., 2010). The reorganization and polymerization of the actin cytoskeleton induce plasma membrane protrusions in the form of lamellipodia and filopodia at the leading edge. Concurrently, plasma membrane contraction at the trailing end, facilitated by active myosin-based motors, generates the force necessary for cell translocation. Moreover, to navigate through the spatially confined brain milieu, glioma cells also deform their nuclei in a myosin II-dependent manner (Etienne-Manneville, 2004).

Efficient transmission of the force, propelling the cell forward, hinges on the establishment of cell-ECM attachments through the transmembrane cell receptors like CD44 and integrins (Mair et al., 2018). Integrins play a crucial role as pivotal connectors bridging the ECM with the intracellular cytoskeleton (Sun et al., 2016). They facilitate adhesion to ECM components present in the vasculature basement membrane, including collagen, fibronectin, and laminin. Conversely, CD44 takes on the responsibility of attaching to the HA-abundant ECM within the brain parenchyma (Kim & Kumar, 2014). These adhesive interactions enable the exertion of traction forces on the ECM, facilitating the forward movement of the cell body. Glioblastoma tumors exhibit marked overexpression of integrin receptors, specifically αvβ3 and αvβ5 (Ellert-Miklaszewska et al., 2020). The signaling pathways activated through these integrin receptors play a important role in orchestrating the localization of proteases responsible for degrading the ECM at the tumor invasion front such as MMPs, uPA, as well as

disintegrin and metalloproteinases (Adams & Gallo). For instance, the expression of αvβ3 is notably associated with elevated levels of MMP-2 in invasive glioma cells (Malric et al., 2017). On the contrary, the correlation between CD44 expression and glioma invasiveness is not direct. It has been demonstrated that glioma migration speed exhibits a biphasic dependence on CD44 expression: it enhances GBM migratory capacity up to a certain threshold (Mair et al., 2018). Apart from its role as an ECM receptor, CD44 is also implicated in GBM stem-like phenotype and resistance to radiation (Wang et al., 2018).

2.3 The Role of Tumor Microenvironment in GBM

GBM cells do not exist in isolation; rather, they reside within a complex and unique microenvironment, with which they closely and continuously interact. The GBM TME is highly diverse and is composed of stromal cells (e.g, astrocytes, endothelial cells and macrophages) as well as non-cellular components, including ECM (Brandao et al., 2019; Sharma et al., 2023; Tamai et al., 2022). GBM cells interact with their TME by either direct cell-cell and cell-matrix interactions, or through paracrine signaling. (Brandao et al., 2019). These multidirectional interactions between GBM cells and their TME play a critical role in GBM progression. In fact, many research studies suggests that GBM cells exploit microenvironmental constituents by functionally and phenotypically transforming them to promote their own survival, proliferation and migration (Zhang et al., 2020).

Accounting for almost 20% of the total brain's volume, the ECM of the brain plays a central role in shaping the environment of the GBM. In contrast to ECM of other tissues, the ECM of the brain consists of a unique mixture of glycoproteins (e.g.,fibronectin, laminins, and tenascins), GAGs represented by HA, and proteoglycans(e.g, aggrecan, neurocan, versican and phosphacan) (Rauti et al., 2020). Conversely, the brain exhibits minimal expression of fibrillar collagens, specifically collagen I. Other integrin-binding proteins, such as fibronectin, laminin, and collagen IV are predominantly localized at the basement membrane of the brain vasculature (Cieśluk et al., 2022).

The GBM TME is distinguished by an overexpression of some ECM components, including HA, tenascins, fibronectin and collagen (Mohiuddin & Wakimoto, 2021). Although astrocytes and oligodendrocytes are the primary sources of ECM components in the brain, it is important to recognize that GBM cells themselves express specific matrix components that facilitate their invasive behavior. As an example, GBM and high-grade gliomas overexpress HA and HAS2, an enzyme responsible for the production of the HA (Valkonen et al., 2018). The effect of HA-receptor interactions on GBM migration depends on the molecular weight of HA; low-molecular-weight HA promotes tumor invasion, whereas high-molecular-weight HA reduces it (Tian et al., 2013).

Apart from the biochemical composition, the mechanical properties of the ECM (e.g., stiffness and matrix density) are also important factors affecting the GBM migration. GBM tumors demonstrate an elevated elastic modulus, twice of that of the healthy brain (Wolf et al., 2019). This elevated stiffness arises primarily from the overexpression of ECM components within the TME, similar to other cancer types. It is noteworthy that the elastic modulus of GBM tumors exhibits significant variation across different tumor regions. Specifically, the necrotic core of the GBM tumor demonstrates the lowest elastic modulus, measuring approximately 0.1 kPa, whereas the densely populated pseudopalisade/infiltrating rim region exhibits a significantly higher elastic modulus of around 10 kPa (Ciasca et al., 2016) .

2.4 Astrocytes in Healthy Brain and in GBM

One of the main cellular components of the GBM TME are astrocytes. Astrocytes are the glial cells of the CNS with a distinctive star-shaped morphology, comprising around 50% of the total human brain cell population (Brandao et al., 2019). They are implicated in a wide range of critical physiological functions both in the developing and the adult human brain. During brain development, astrocytes balance the formation and elimination of neuronal circuits (Fossati et al., 2020). Astrocytes release specific proteins, such as thrombospondins, glypicans, and hevins, that contribute to synaptogenesis and engulfment of synaptosomes. In addition, astrocytes provide

molecular cues that guide the migration of developing axons and certain neuroblasts to their designated locations within the developing brain (Vasile et al., 2017). In the adult brain, astrocytes mediate the balance between excitation and inhibition by reuptaking neurotransmitters from the synaptic cleft through different transporters, including GLAST and GABA transporters (GAT-1) (Nieland et al., 2021). Furthermore, astrocytes modulate the BBB integrity by ensheathing vasculature and directly communicating with endothelial cells and pericytes (Daneman & Prat, 2015). Through these interactions, astrocytes contribute to the amino acid, water and ionic homeostasis of the brain. Astrocytes also establish a critical interface between neurons and blood vessels in the brain that regulates the blood flow to regions of heightened neuronal activity via the process known as neurovascular coupling. This function is attained by adjusting the vascular dilation level and serves to ensure that active brain regions are supplied with sufficient oxygen and nutrients (Filosa et al., 2016).

Apart from being essential for healthy brain homeostasis, astrocytes are now recognized as key contributors to various brain disorders characterized by abnormal synaptic function and neuronal death, including Alzheimer’s, Huntington's,Parkinson's disease, and amyotrophic lateral sclerosis (Brandebura et al., 2023). In response to brain injury and inflammation, astrocytes undergo a remarkable transformation into reactive astrocytes, a process known as astrogliosis. This transformation is accompanied by a complex cascade of morphological and transcriptional changes, including the hypertrophy of the astrocytic cell bodies, increased proliferation rate at the lesion site, and upregulation of key members of astrocytic intermediate filaments such as GFAP, nestin, and vimentin (Brandao et al., 2019). In addition, reactive astrocytes release growth factors(e.g., BDNF,cytokines(e.g., CCL2, IL-6), and ECM components(e.g., collagens, versican). The overexpression of GFAP is considered to be the hallmark of astrocyte reactivity (Zhang et al., 2020). Through this process, reactive astrocytes act as a crucial line of defense, working to restore homeostasis in the damaged CNS by physically isolating lesions, providing metabolic support to damaged neurons, regulating blood-brain barrier permeability, and remodeling the ECM and synapses (Zhang et al., 2020).

Reactive astrogliosis is also elicited in the context of GBM, as the malignant growth of GBM tumors brings about the invasion and destruction of adjacent brain tissue. While initially aimed at impeding tumor growth and safeguarding the surrounding

healthy brain tissue, the astrogliosis at advanced stages of tumor development results in the emergence of TAAs that ultimately aids the tumor progression (Henrik Heiland et al., 2019).

2.5 In-vitro Co-culture Studies Investigating the role of Astrocytes in GBM Invasiveness and Migration

As it was highlighted in previous sections, the diffusive nature of invasion into the surrounding brain parenchyma is the hallmark feature distinguishing GBM tumors as highly aggressive and treatment resistant. While in-vivo studies offer valuable insights into the mechanisms of GBM migration by containing the heterogeneous milieu of the TME, they are often characterized by their complexity, time-consuming nature, high cost, and limited reproducibility. In addition, due to the high level of diversity within the GBM TME, it is challenging to dissect the individual contributions of each component to glioma invasiveness in animal studies (Chekhonin et al., 2018). On the other hand, despite their simplified nature, in-vitro models enable focusing on the direct interactions between GBM tumors and their TME constituents. Therefore, in-vitro models offer a more potent tool for elucidating the exact signaling pathways governing GBM invasion.

Several in-vitro co-culture studies have focused on investigating the impact of TAAs on the migratory and invasive behavior of GBM cells. One common and notable finding of these studies was that TAAs increase GBM invasiveness through the upregulation of MMPs (Kieseier et al., 1999). Le et al. demonstrated that high numbers of TAAs found in the vicinity of glioma tumors enhance the transmigration of U251 glioma cells by mediating the activation of MMP-2 through the urokinase-type plasminogen activator (uPA)-plasmin cascade (Le et al., 2003). It was shown that in the co-culture system, uPA secreted by both cell types gets activated and converts plasminogen released by glioma cells into plasmin. Subsequently, the plasmin facilitates the cleavage and activation of pro-MMP-2 released by astrocytes. This finding sheds light on the intricate interplay between TAAs and GBM cells, implicating the uPA-plasmin cascade as a significant mediator of MMP-2 activation and subsequent glioma

cell migration. Similarly, Gagliano et al. used a transwell co-culture system to investigate the effect of glioma cells on astrocytic reactivity and malignant transformation (Gagliano et al., 2009). They also confirmed that the presence of glioma cells augments the reactivity of astrocytes, as evidenced by the upregulation of GFAP and the secretion of MMP-2.

Chen et al. revealed another signaling cascade of astrocyte-glioma communication, the IL-6 and MMP14 axis, that contributes to the increased migration of GBM cells in the presence of astrocytes (Chen et al., 2016). MMP-14 or membrane type 1 MMP(MT1-MMP) is a transmembrane member of MMPs that becomes activated by integrin clustering at the leading edge of a migrating glioma cell, an event preceding and being necessary for the activation of soluble proteases (e.g., MMP-2 and MMP-9). In this study, human astrocytes co-cultured with glioma cell lines in a transwell format upregulated the secretion of the cytokine IL-6. The paracrine stimulation of glioma cells with IL-6 promoted MMP-14 expression, which in turn mediated MMP-2 activity, responsible for the augmented invasion potential of glioma cells. Li et al. provided additional support for the association between IL-6 secretion and MMP-2 activity in GBM cells (Li et al., 2010). They demonstrated that exposing glioma cell lines to the IL-6 cytokine leads to elevated levels of the STAT3 transcription factor, which directly enhances MMP-2 production by binding to its gene promoter.

Rath et al. also reported that astrocytes co-cultured with glioma stem cells (GSC) upregulate the secretion of IL-6, IL-8, TGF-β and VEGF cytokines and growth factors, which results in increased in-vitro invasiveness of CD133+ GSC (Rath et al., 2013). Furthermore, the markers of tumor aggressiveness (e.g., CD44, CCL2 and Has2) were overexpressed in the presence of astrocytes or astrocyte-conditioned medium.

The elevated expression of IL-6 has been linked to the poor prognosis and the highly aggressive mesenchymal transformation observed in GBM (West et al., 2018) (Senft et al., 2011). Within the tumor TME, IL-6 acts by activating the JAK/STAT signaling pathway through binding to either soluble or membrane-spanning receptors, IL-6Rs (Johnson et al., 2018). The binding of IL-6 to its receptors triggers their dimerization, which in turn activates JAK tyrosine kinases. This leads to the phosphorylation of IL-6Rs at multiple locations, which serve as docking sites for STAT3 monomers. These recruited STAT-3 monomers are also phosphorylated by JAKs and form dimers, leading to their activation and nuclear translocation. Finally, the

STAT3 transcription factor promotes GBM angiogenesis and invasiveness by mediating the expression of VEGF and MMPs (West et al., 2018).

Another important mediator of the astrocyte-glioma crosstalk is the p53 pathway. The p53 gene functions as a tumor suppressor, preventing the proliferation of damaged cells by inducing cell cycle arrest and programmed cell death (apoptosis) in response to stress signals (Biasoli et al., 2014). Biasoli et al. reported that exposing astrocytes to glioma-conditioned medium results in the blocked expression of p53 by astrocytes. The p53+/- astrocytes in turn alter their ECM composition, by enhancing the secretion of ECM components, laminin and fibronectin, which induces the invasive mesenchymal phenotype in adjacent glioma cells. The EMT transformation of glioma cells is confirmed by their upregulation of mesenchymal associated proteins (vimentin and N-cadherin) and downregulation of epithelial markers (E-cadherin and sprouty 2).

2.6 GelMA hydrogel as a 3D Culture System for Modelling GBM Microenvironment

Despite providing invaluable mechanistic insights into the role of TAAs in GBM migration, 2D models exploited in studies described in the previous section fail to capture the composition and mechanical properties of the GBM ECM. The ECM, a complex network of proteins and other molecules, plays a crucial role in determining the native phenotype and behavior of GBM cells (Mohiuddin & Wakimoto, 2021). Inherent to 2D culture conditions, cells grown in such settings often exhibit distinct responses compared to their native counterparts. For example, cells grown in 2D conditions often possess an aberrant polarization, flattened morphology, which in turn may alter their signaling pathways and skew the interpretation of experimental results, particularly when assessing the efficacy of pharmaceutical interventions (Caliari & Burdick, 2016; Saraswathibhatla et al., 2023).

On the other hand, embedding cells within 3D matrices offers distinct advantages by facilitating the establishment of relevant cell-cell and cell-matrix interactions. In addition to biochemical interactions, 3D cultures permit the formation of gradients of soluble cues, such as oxygen and growth factors, which are critical for

cellular function and migration (Habanjar et al., 2021). Furthermore, growing cells in a 3D configuration spatially confines them, requiring cells to either enzymatically remodel the ECM or mechanically deform it in order to spread and migrate (Caliari & Burdick, 2016). This behavior closely mirrors the behavior exhibited by cells in their native environments. Considering the complexity and importance of GBM TME, it is imperative to develop systems incorporating 3D matrices that mimic the tumor ECM. The development of these systems holds great potential for enhancing our understanding of the role of TME in GBM progression and bridging the gap between 2D drug trials and animal studies.

The field of biomaterials has advanced to provide a range of materials with a high level of biomimicry and some level of control over their mechanical and compositional properties (Wolf et al., 2019). Among them, hydrogels emerged as promising candidates for mimicking the low-stiffness, well-hydrated ECM of the brain. Hydrogels are 3D networks composed of crosslinked hydrophilic polymers that have the ability to absorb and retain water, causing them to swell and increase in volume (Yue et al., 2015). Hydrogels based on naturally occurring materials are advantageous due to providing cell-responsive cues and being biodegradable. However, they are usually deficient in mechanical strength and tunability, and suffer from batch-to-batch variability. For example, widely used Matrigel, derived from mouse sarcoma and containing basement membrane proteins, has a poorly defined chemical composition and a high batch-to-batch variability(Aisenbrey & Murphy, 2020). Another very popular natural hydrogel, collagen undergoes temperature-based gelation, offering a poor control over its crosslinking time and density. Most importantly, both of these biomaterials are not suitable for mimicking the nanoporous, highly hydrated brain ECM, due to possessing fibrous architecture and being rich in collagen (Wolf et al., 2019).

Photocrosslinkable gelatin with substituent methacryloyl groups (GelMA) offers advantages of both natural and synthetic hydrogels. Being derived from denatured collagen 1, gelatin retains its cell-binding arginine-glycine-aspartic acid (RGD) and MMP-degradable motifs required for cell attachment and matrix remodeling (Yue et al., 2015). Gelatin is capable of thermal crosslinking; however, this process is characterized by slow crosslinking kinetics and limited control over the final gel properties (Klotz et al., 2016). The introduction of methacryloyl groups to the gelatin

backbone enables GelMA to undergo photocrosslinking upon the addition of a PI under specific UV wavelengths (Bupphathong et al., 2022). This unique property of GelMA grants a greater control over the temporal and spatial aspects of its cross-linking kinetics. Moreover, by manipulating variables such as the degree of methacrylation, hydrogel concentration, UV intensity, and exposure time, parameters including hydrogel porosity and stiffness can be adjusted accordingly (Yue et al., 2015). Additionally, the incorporation of specific ECM components such as HA further enhances GelMA's tissue specificity and biomimicry (Nemeth et al., 2014)

3

MATERIALS AND METHODS

3.1 Cell Culture

U87 and immortalized normal human astrocyte (I-NHA) cell lines were a kind gift from Dr. Tuğba Bağcı Önder (Koç University School of Medicine, Istanbul). Both cell types were cultured in DMEM HG (Sigma Aldrich) with 10% FBS(Biowest), 1% penicillin-streptomycin (Biowest). Cells were maintained at 37°C in a humidified atmosphere of 5% CO2 and passaged at 80-90% confluence.

3.2 Coating of Glass Slides

In order to facilitate the adhesion of GelMA constructs, 18x18 mm glass coverslips were functionalized with TMSPMA (Sigma-Aldrich, Cat. No. 440159). The glass slides were first immersed in a 10% (w/v) sodium hydroxide solution (Merck, Germany) for 1.5 hours to activate the glass surfaces, generating silanol groups. Subsequently, the glass slides were rinsed three times with distilled water and then dried in an oven at 60°C for 0.5-1 hour. Following this, the glass slides were treated with TMSPMA at 80°C overnight and further rinsed with absolute ethanol. To ensure sterility, the glass slides were briefly washed with 70% ethanol and were maintained inside the UV light within a laminar flow hood. The treated glass slides were kept in the hood and used within one week after coating.

3.3 GelMA Synthesis

GelMA (ZetaMatrix) was synthesized by utilizing the one-pot method as described previously (Shirahama et al., 2016). In short, 10% (w/v) of gelatin solution was prepared by dissolving 10 g of bovine skin gelatin in 100 ml of carbonate-

bicarbonate buffer (0.25 M, pH 9) at 50°C. It was followed by a gradual dropwise addition of MA with simultaneous magnetic stirring at 50°C. For the reaction termination to occur, the pH of the solution was adjusted to 7.4. After, the solution was dialyzed against distilled water for 7 days at 40 °C using a dialysis membrane to remove unreacted MA groups and salts. This was followed by lyophilization and storage at -20°C.

3.4 Scanning Electron Microscopy (SEM)

The surface morphology and microstructures of GelMA constructs were observed via FE-SEM (Zeiss Ultra Plus, Bruker, MA). Hydrogel constructs were fabricated through photolithography via photomasks and left to swell in DPBS for 1-2 hours. After careful DPBS aspiration, gels were briefly washed with a deionized water and transferred to -20 C for 2 hours. Later, they were transferred to -80 C and stored overnight. Finally, samples were lyophilized for 24 hours, dislodged from the surface of glass slides, and mounted on SEM stubs with double-sided carbon tape. After sputter coating the samples with gold for 45 seconds, they were imaged at EHT of 3kV with a working distance of 6 mm. The pore sizes were measured with ImageJ.

3.5 Rheology Measurements of GelMA Storage Modulus

The rheological properties of a 5% (w/v) GelMA hydrogel with a 1% (w/v) Irgacure PI concentration were assessed using a Rheometer (TA Instruments, Delaware, USA), equipped with a UV light attachment. Prior to measurement, all hydrogel samples were stabilized at 37 °C. For the in-situ crosslinking process, 100 μL of the GelMA prepolymer solution was loaded onto the rheometer's parallel plate, which was set with a gap size of 300 μm. This setup was then exposed to UV light at a power of 30 mW to initiate crosslinking. The crosslinking behavior of the hydrogel, specifically its loss modulus (G") and storage modulus (G'), was monitored in real-time over a duration of 5 minutes. This monitoring was conducted using the time sweep oscillatory mode of the rheometer. During this process, a constant strain amplitude of 10% was maintained,

and the frequency was set at 5 Hz, ensuring that the measurements were taken within the hydrogel's linear viscoelastic region.

3.6 GelMA Prepolymer Solution Preparation

The prepolymer solution of GelMA was prepared by reconstituting lyophilized GelMA in DPBS (Biowest,L0615) containing the PI,2-Hydroxy-4′-(2-hydroxyethoxy)-2-methylpropiophenone (Irgacure 2959). Initially, the PI solution was prepared by dissolving Irgacure 2959 powder in the desired volume of DPBS at 80°C, resulting in a 1% (w/v) concentration. Subsequently, the lyophilized GelMA was added to the Irgacure 2959 solution to achieve a final concentration of 5% (w/v) GelMA prepolymer solution. The mixture was maintained at 37°C while being intermittently vortexed to ensure the complete and uniform dissolution of both components. Following this, the mixture was filtered through a 0.2 µm filter and utilized for subsequent cell encapsulation studies. For cell encapsulation, U87 or NHI cells were trypsinized with 0.25% Trypsin/EDTA (Wisent)**,** counted, and the required number of cells was pelleted through centrifugation at 300 g for 5 minutes. Subsequently, the pellet was resuspended in the corresponding volume of 5% (w/v) GelMA prepolymer solution to yield varying concentrations of cell suspensions (1,2,3 mil/ml).

3.7 The Fabrication of GBM TME Model via Two-Step Photolithography

The fabrication of the micropatterned model was accomplished through a two-step photolithography, a process that enables the creation of precise patterns of a light-sensitive hydrogel, GelMA, through the UV light exposure. In the first step of the microfabrication process, 20 µL of the GelMA pre-polymer solution containing dispersed cells was dispensed onto a spacer with a depth of 0.3 mm. The depth of the spacer could be adjusted to achieve the desired thickness of the hydrogel constructs. Subsequently, TMSPMA-coated coverslips were inverted on the top of the deposited pre-polymer drop to evenly spread it and fill the spacer depth. A doughnut-shaped photomask (designed with CorelDRAW software, Corel corp., Canada and printed by A Print, Izmir) was placed on the top of the glass slide and exposed to UV light (power

density of 6,25 W/cm^2,) for 25 seconds by using OmniCure S2000 UV 12 Light Curing System (Excelitas Technologies Corp., Waltham, MA, USA). The UV device probe was positioned at a 40 mm distance from the microfabrication stage. The UV exposure was followed by DPBS washing to remove the uncrosslinked pre-polymer solution, revealing an array of cell-laden doughnut patterns. Patterned glass slides were transferred to a 6-well plate and stored in 1 mL of DPBS until the second step of the fabrication process. In the second step, 13 µL of pristine GelMA was pipetted onto the spacer of the fabrication platform, and the patterned glass slide was inverted on top, ensuring uniform spreading and filling of the spaces between the doughnut patterns with pre-polymer solution. This assembly was exposed to UV light for additional 15 seconds to cure the gel surrounding doughnuts. Finally, micropatterned gel constructs were washed one more time with DPBS and cell culture medium, followed by addition of 2 ml of cell culture medium to each well of the 6 well plate. Cell medium was replenished every three days.

After optimizing the two-step photolithography microfabrication protocol for only GBM cells line, it was adapted for co-culture studies of U87 cells with immortalized astrocytes (I-NHA). The flexibility of this method allowed us to co-culture cells in two distinct configurations by precisely localizing them. The first configuration called direct co-culture involved the incorporation of both cell lines into doughnut-shaped constructs. This was achieved through the photocrosslinking of a GelMA pre-polymer solution containing U87 and I-NHA cells at a ratio of 3:2 (3mil/ml and 2mil/ml respectively) with a total cell concentration of 5mil/ml. The resulting doughnuts, which contained co-culture of U87 GBM cells and immortalized astrocytes in direct contact with each other, were surrounded with a matrix of pristine GelMA by following the two-step photolithography protocol described above. The second configuration entailed the creation of U87 doughnuts with 3mil/ml concentration surrounded by an astrocyte-dispersed matrix of 2mil/ml density. To pattern cells in this layout, the second step of the photolithography process was modified and involved inverting U87 doughnuts on astrocyte-dispersed drop of GelMA. As a result, U87-encapsulating microspheres were encircled with a matrix of evenly distributed I-NHA of the same height.

3.8 Cell Viability Assays

MTT colorimetric assay was utilized to assess the metabolic activity of encapsulated U87 and NHI cells across different seeding concentrations. Briefly, 0.5 mg/ml of MTT solution was prepared by diluting MTT (Invitrogen, Cat. No. M6494) stock solution (5mg/ml) in the appropriate volume of serum-free cell culture medium. Then, 2 ml of the MTT solution was dispensed to each well of the 6-well plate containing a gel construct and incubated in the dark at 37°C for 4 hours. Following the 4-hour incubation, the cell culture medium was carefully aspirated from each well, and 1 ml of a DMSO solution (PanReac AppliChem, Cat. No. A3672) was added to dissolve the formazan crystals. To ensure thorough dissolution of all crystals within the gel constructs, the 6-well plate was placed on a shaker for 30 minutes. Once the crystals were completely dissolved, 200 µl of solution was transferred into the wells of a 96-well plate, and the absorbance values of each well were read with a plate-reader (BioTek, Synergy H1 Hybrid Reader) at 570 nm with a reference wavelength of 690 nm. Each cell concentration had three experimental replicates which were averaged per experiment.

For Live/ Dead assay, the Cyto3D® Live-Dead Assay Kit (The Well Bioscience) was used to stain live and dead cells on Days 1,4, and 7. The kit was composed of acridine orange (AO) and propidium iodide (PI), staining all nucleated cells and dead cells, respectively. Briefly, 20 µl of the ready to use kit was added to the cell-laden hydrogel constructs and incubated for 5 minutes. Due to the quenching, all live nucleated cells produced green fluorescence, while the dead ones fluoresced red. The images were taken with the confocal microscope (Leica, DMI8 SP8).

3.9 Phalloidin Staining of U87 Cytoskeletal Organization

To visualize the F-actin cytoskeletal organization of encapsulated U87 GBM cells, phalloidin staining was used. Cell-laden hydrogel constructs were washed 3X with DPBS and fixed with 4% (w/v) PFA solution in DPBS for 30 minutes. Later, the hydrogels were washed 2X with 0.3M glycine-DPBS for 3 minutes each wash and 1X with DPBS. The samples were permeabilized with 0,1% (v/v) Triton-X in DPBS and blocked with 3% BSA(Capricorn) for 1 hour at the room temperature. A 1:1250(v/v)

dilution of Alexa Fluor®488 Phalloidin (Abcam, Cat. No. ab176753)(200µl) was added to the blocked sample and incubated for 45 minutes. Once stained against F-actin, cells were counterstained for their nuclei by adding 1 ml of Hoechst (Thermo Scientific, Cat. No. 62249) (1:1000) solution diluted in DPBS.

3.10 RNA Extraction from Hydrogel Constructs

The RNA isolation was performed by the slight modification and adaptation of the previously described protocol (Loessner et al., 2016). Firstly, cell-laden hydrogels were washed with DPBS and manually dislodged from glass slides by using a 20ul pipette tip. Next, the lysis solution made of 1%(v/v) β-mercaptoethanol(Sigma Aldrich, Cat. No. 21985023) and RA1 lysis buffer was added to each construct. This was followed by a thorough pipetting to facilitate the further disruption of gels. For the sufficient retrieval of RNA, 3-5 hydrogel constructs per each experimental condition were pooled inside a cryovial. To ensure the homogenization of constructs, the cryovial with the lysate was snap-frozen in the liquid nitrogen. Subsequently, frozen samples were thawed at room temperature and mechanically lysed by passing through a 20-gauge needle with 2.5-ml syringe 18-20 times. The lysates were transferred to spin columns and the RNA extraction was proceeded following the manufacturer's instructions for NucleoSpin RNA, Mini kit for RNA purification (Macherey-Nagel,Cat.No: 740955). The purity and concentration of RNA were determined by Thermo Scientific™ NanoDrop™ 2000/2000c Spectrophotometer. For cDNA synthesis, 150ng of RNA was converted into cDNA using M-MLV Reverse Transcriptase (Invitrogen, 28025013).

3.11 Gene Expression Analysis by Real Time Quantitative PCR (RT-qPCR)

qPCR experiments were performed by LightCycler® 480 II Real-Time PCR System (Roche, Germany). Briefly, a reaction volume of 20µL, consisting of 18µl master mix solution (10µl of LightCycler® 480 SYBR Green I Master (Roche, Germany); 7µl of Nuclease-free water; 1µl of primer solution) and 2µL of cDNA was

loaded to each well of 96-well plate. Target gene expression levels were determined by ΔΔCt method, normalizing to housekeeping gene β-actin. The primer sequences are listed in the table.

Table 1. Primer Sequences used for qPCR

Gene	Primer Sequence 5'-3'
MMP-2	GATACCCCTTTGACGGTAAGGA
	CCTTCTCCCAAGGTCCATAGC
MMP-3	AGGCAAGACAGCAAGGCATA
	GATATTTCTGAACAAGGTTCATGC
MMP-9	TTGACAGCGACAAGAAGTGG
	GCCATTCACGTCGTCCTTAT
MMP-14	TCAACCCAGGACTACCTCCC
	CAGCGCTCCTTGAAGACAAAC
VEGF	CTACCTCCACCATGCCAAGT
	GCAGTAGCTGCGCTGATAGA
HIF-1α	TGATTGCATCTCCATCTCCTAC
	GACTCAAAGCGACAGATAACACG
TGF-β	GCCTTTCCTGCTTCTCATGG
	TCCTTGCGGAAGTCAATGTAC
IL-6	TGAACTCCTTCTCCACAAGCG
	TCTGAAGAGGTGAGTGGCTGTC
Fibronectin	GGTGACACTTATGAGCGTCCTAAA
	AACATGTAACCACCAGTCTCATGTG
CD44	CTGCCGCTTTGCAGGTGTA
	CATTGTGGGCAAGGTGCTATT
ACTB	GACAGGATGCAGAAGGAGATCAC
	GCTGATCCACATCTGCTGGAA

3.12 GFP and RFP tagging of U87 and I-NHA Cells Lines

For RFP and GFP labeling of U87 and I-NHA cells lines, respectively, lentiviral mediated transduction was used. HEK-293T cells were used to package pLenti CMV GFP Puro plasmid(Addgene # 17448) and Plenti-CMV-MCS-RFP-SV-puro(Addgene #109377) plasmids using cotransfected psPAX2 and pMD2.G plasmids. Supernatants containing viruses were used for transduction of U87 and I-NHA cells.

3.13 Co-culture Experimental Setups for Gene and Protein Expression Analysis

3.13.1 Co-culture Experimental Setup for qPCR analysis of Gene Expression

For qPCR analysis of the 3D culture effect on gene expressions of U87 GBM cells, cells harvested from one well of 6-well plate (around 500.000 cells) served as a control, while U87 cells grown inside GelMA microspheres comprised the experimental group.

For studies investigating the effect of the astrocyte co-culture on the gene, U87 GBM cells (3mil/ml) directly co-cultured with NHIs (2mil/ml) inside doughnuts comprised the experimental condition. The control group was made by mixing RNA isolated from individually cultured I-NHA of 2mil/ml and U87 of 3mil/ml inside doughnut constructs. The method was inspired by the approach utilized in 3D culture gene expression studies (Cui et al., 2023; Ngo & Harley, 2019).

For qPCR analysis of the co-culture configuration effect on gene expression, the tumor model was treated as a whole system. The total RNA was isolated from directly co-cultured cells and those in the stamping configuration.

3.13.2 Co-culture Setup for Immunofluorescent Staining against GFAP

For co-culture experiments focusing on the impact of U87 GBM cells on the expression of GFAP by I-NHA, the experimental group consisted of doughnuts containing RFP-labeled U87 glioma cells of 3mil/ml density embedded within a surrounding matrix of dispersed astrocytes of 2mil/ml. The control group was

comprised of empty doughnuts, devoid of U87 cells, surrounded by a matrix of suspended astrocytes.

3.14 Image Processing for Migration Analysis

To quantify the cell migration, we calculated the total area of all migrated cells outside the doughnut constructs on Days 3,5,7, and 9 of culture. For image processing, Matlab and its computer vision and image processing libraries were used. Z-stack images of two co-culture configurations on respective days of culture were thresholded to convert them into 2D arrays of binary images. A key step was masking the doughnut areas with a circle of set radius to isolate the area of interest – the cells that migrated outside the circle. By counting the total area of these cells in both pixel square and micrometer square, we could quantify their migration. The migration capacity, was calculated as the percentage of the total area occupied by migrated cells relative to the total frame area of 1024x1024 pixels (Cui et al., 2023).

4

RESULTS AND DISCUSSION

4.1 Characterization of GelMA Mechanical Properties

To gain insights into the crosslinking kinetics of a 5% (w/v) GelMA hydrogel with 1% (w/v) Irgacure PI, rheological experiments were conducted using a rheometer equipped with a UV attachment. The experiments revealed that the stiffness (G') of the 5%(w/v) GelMA exhibited a marked increase within the initial 24-28 seconds of UV exposure, reaching a value of approximately 1500 Pa **(Figure 4.1(A)).** This rapid increase in storage modulus is indicative of a swift crosslinking reaction within the hydrogel after exposure to UV light, inducing a notable enhancement in its mechanical strength. Subsequent to this initial phase, the storage modulus demonstrated a plateau, with only a marginal increase of about 200 Pa over the following 270 seconds of UV exposure. This leveling off of the storage modulus after the first 28 seconds implies that most of the methacryloyl groups in the GelMA hydrogel had rapidly formed covalent bonds during the initial crosslinking phase. The slight increment observed after this period could be indicative of a slower, secondary reaction phase or the approach towards a saturation point, where nearly all the crosslinkable sites have been utilized.

It is noteworthy that both the duration of crosslinking and the maximum storage modulus achieved by our 5% GelMA hydrogel align with findings reported in existing literature (He et al., 2023) . However, due to the utilization of a relatively high Irgacure PI concentration (1%(w/v)), the crosslinking in our hydrogel prepolymer solution was initiated after only 3 seconds of UV exposure, in contrast to 30 seconds for 5% GelMA with 0.25% LAP PI in the referenced study. The literature presents conflicting evidence regarding the toxicity of high PI concentrations. For instance, Xu et al. reported significant toxicity at PI concentrations greater than 0.5% affecting the viability of 3T3 cells (Xu et al., 2020). In contrast, Nguyen et al. found no significant impact of PI concentration on the viability of human epithelial cells of kidney (Nguyen et al., 2019). These varying outcomes suggest that the toxic effects of crosslinking parameters, such

as UV exposure duration, PI concentration, and GelMA's degree of methacrylation, may vary based on cell type. As the next section demonstrates, both U87 and I-NHA cell lines maintained a high level of viability within a one-week period inside GelMA constructs.

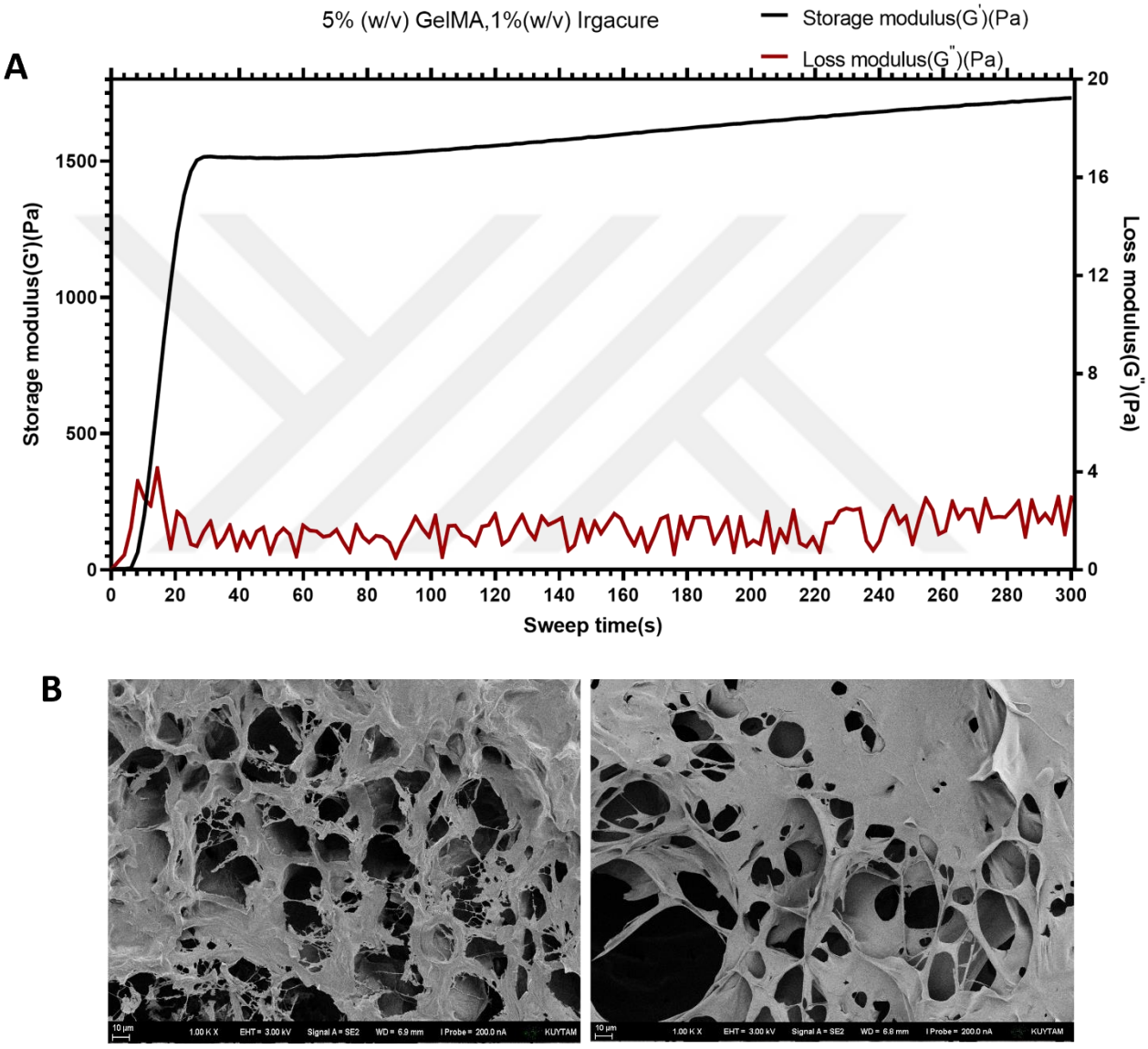

Figure 4.1. Characterization of mechanical properties of 5 % (w/v) GelMA hydrogels.

A) Time sweep profiles of the storage modulus (G') showing a drastic increase in stiffness within 30 seconds of UV exposure

B) Representative SEM micrographs demonstrating the spongy network of interconnected pores. The average pore size is 22 µm. Bar signifies 10 µm.

4.1 Viabilities of U87 GBM and I-NHA Cell Lines inside GelMA Constructs

4.1.1 Quantitative Assessment of the Cell Concentration Impact on Cell Viability

After conducting the mechanical characterization of the 5% GelMA hydrogel, the subsequent critical optimization step involved assessing cell viability. GelMA is a hydrogel known for its excellent cytocompatibility, having been successfully utilized for culturing various cell types, including primary normal cells, stem cells, and cancer cell lines, with consistently high cell viability rates (He et al., 2023). Despite GelMA's established cytocompatibility, the unique parameters of our microfabrication setup necessitated specific adjustments for optimal cell viability. These parameters include a defined UV power (6,25 W) with a separation distance of 40 mm from the microfabrication stage, a 1% (w/v) Irgacure concentration, a 25-second UV exposure duration, and the utilization of photomasks in the fabrication process.

To ensure the compatibility of the developed hydrogel system with U87 and immortalized normal human astrocytes(I-NHA) cell lines, we encapsulated three different concentrations of both cell types (1 million/ml, 2 million/ml, and 3 million/ml) within GelMA doughnut constructs. The viabilities of these different cell concentrations were assessed quantitatively using the MTT colorimetric assay. In MTT assay, the colorimetric change is induced by the cellular metabolic activity that reduces soluble tetrazolium MTT component into insoluble formazan crystals (Mahajan et al., 2012). The enzymatic reduction of MTT is dependent on the mitochondrial respiration of the cell, and is induced by the mitochondrial enzyme, succinate dehydrogenase (CHACON et al., 1997).

Upon careful examination of **Figure 4.2(A)**, it is evident that I-NHA cells, across all three concentrations, demonstrated a notable increase in cell viability at Day 4 compared to Day 1 of culture. The concentration of 2mil/ml witnessed an almost two-fold increase in the cell viability, comprising the cell concentration with the highest percent viability through the 4-day culture period ($p < 0{,}0001$). In contrast, 3 mil/ml concentration showed a significantly less percent viability when compared to both 1mil/ml and 2mil/ml($p = 0{,}0169$ and $p = 0{,}0008$, respectively). Reduced cell viability of I-NHA at a higher density can be attributed to the limited diffusion of oxygen and nutrients as well as the high metabolic demand of cells. Oxygen and soluble cue

gradients form naturally within 3D hydrogels as a function of gel thickness(Schmitz et al., 2022). Therefore, the compromised cell viability at a higher cell density of 3mil/ml may be explained by the oxygen and nutrient diffusion limit and the resulting hypoxia, specifically towards the center of gel constructs. Based on the results of the MTT assay, 2mil/ml cell concentration was utilized for further co-culture studies.

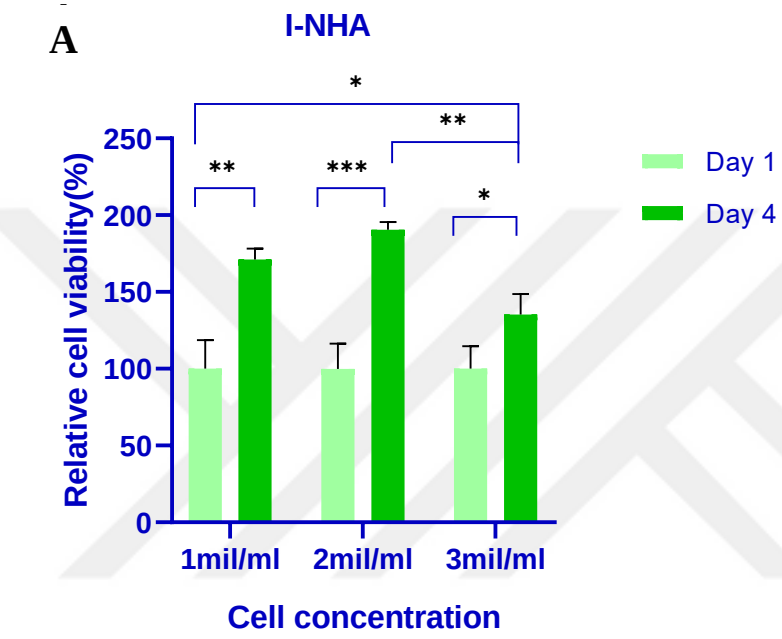

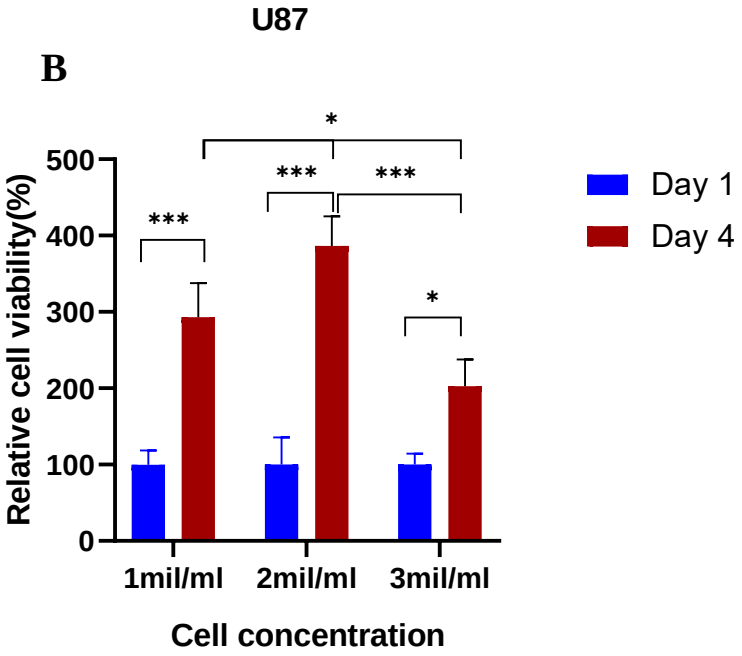

Figure 4.2. The impact of cell concentration and culture duration on the viability of I-NHA and U87 cells within GelMa constructs. *Cell metabolic activity at different concentrations (1 million/ml, 2 million/ml, 3 million/ml) was quantified using the MTT assay. Absorbance values measured at Day 4 of culture were normalized to those at Day 1. All values signify the mean ± standard deviation of three biological replicates.* ***A)*** *On Day 4 of culture, I-NHAs at concentrations of 1 million/ml and 2 million/ml demonstrated significantly higher percent viability compared to 3 million/ml cell density (p=0.0169 and p=0.0008, respectively).* ***B)*** *U87 displayed a comparable pattern, where 2mil/ml exhibited a four-fold increase in viability, significantly surpassing both 1 million/ml and 3 million/ml concentrations (p=0,0139 and p<0,0001, respectively).*

When it comes to U87 cell line **(Figure 4.2(B)),** there has also been a marked rise in viability for all three different concentrations (p<0,001 for 2mil/ml and 1mil/ml, p=0,0072 for 3mil/ml), with the 2 mil/ml group having the highest increase of four times through a 4-day period. This value was significantly higher when compared to those of 1mil/ml and 3mil/ml concentration groups (p=0,0139 and p<0,0001, respectively). Importantly, the percent viability changes of U87 cell line were approximately twice as much as those of I-NHA cells for all three different concentrations. The 3 mil/ml concentration group showed the lowest normalized percent viability, reaching the value of only 200%.

Despite this finding, 3mil/ml concentration has been selected for further studies due to a number of reasons. Encapsulating a denser cancer cell population within the 3D hydrogel promotes hypoxia, a characteristic already inherent in 3D hydrogel systems. The resulting scarcity of dissolved oxygen and low pH within the hydrogel mirrors conditions found in the tumor core interstitial fluid, thereby fostering necrosis, and encouraging a more invasive and pro-angiogenic phenotype in cancer cells (Monteiro et al., 2017). The accumulation of HIF-1α due to hypoxia was shown to enhance glioma invasion through the activation of Notch or PI3K/Akt/mTOR pathways (Qiang et al., 2012). As the focus of this thesis study is the GBM migration, 3mil/ml was selected for further experiments. The findings of this thesis provide additional support for the rationale behind choosing the 3 mil/ml cell concentration. Notably, this concentration resulted in a more extensive invasion of the surrounding GelMA matrix compared to the

2 mil/ml concentration **(Figure A.1).** Furthermore, the 3 million/ml cell concentration induced the formation of agglomerates resembling cancer spheroids to a greater extent when compared to the 2 million/ml cell concentration by Day 7 of culture.

4.1.2 Qualitative Evaluation of the Culture Duration on Cell Viability via Live/Dead Assay

The Live/Dead assay images **(Figure 4.3)** obtained for both cell types over the one-week period illustrate excellent viability of cells within the GelMA constructs. Initially, at Day 1, a relatively high number of dead cells stained with propidium iodide (PI) was observed for both U87 and I-NHA cells, potentially due to the immediate stress induced by the microfabrication process and the new environment. However, by Day 4, cells adapted and exhibited enhanced proliferation, as evidenced by most cells stained in green. Notably, by Day 7, dead U87 cells, marked in red, accumulated in the center of doughnuts, a phenomenon not observed in I-NHA cells. One potential explanation for the accumulation of dead cells in the center is that U87 cells, characterized by higher concentrations and a rapid proliferation rate, compete for nutrients and oxygen. While most cells experiencing hypoxia migrate outside the doughnuts, those in the center do not have the opportunity to do so, resulting in their entrapment and subsequent accumulation of dead cells. This scenario mimics the formation of dead cells resembling necrotic cells found in the hypoxic core of tumors in vivo within our experimental platform (Wolf et al., 2019).

The Live/Dead images **(Figure 4.3)** also allow for the visual comparison of morphologies and migration behaviors of the two cell types inside the doughnuts. At Day 1, both U87 and I-NHA cells exhibited a round morphology, as they had not yet have time for establishing cell-matrix interactions and GelMA hydrogel remodeling. By Day 4, U87 cells formed regions of high cell densities at the doughnut edges, resembling pseudopalisades – a histopathological feature characteristic of GBM tumors. By Day 7, this feature became more pronounced, and U87 cells extensively migrated outside the doughnuts. In contrast, I-NHA cells did not exhibit migration but instead established extensive networks within the GelMA doughnut.

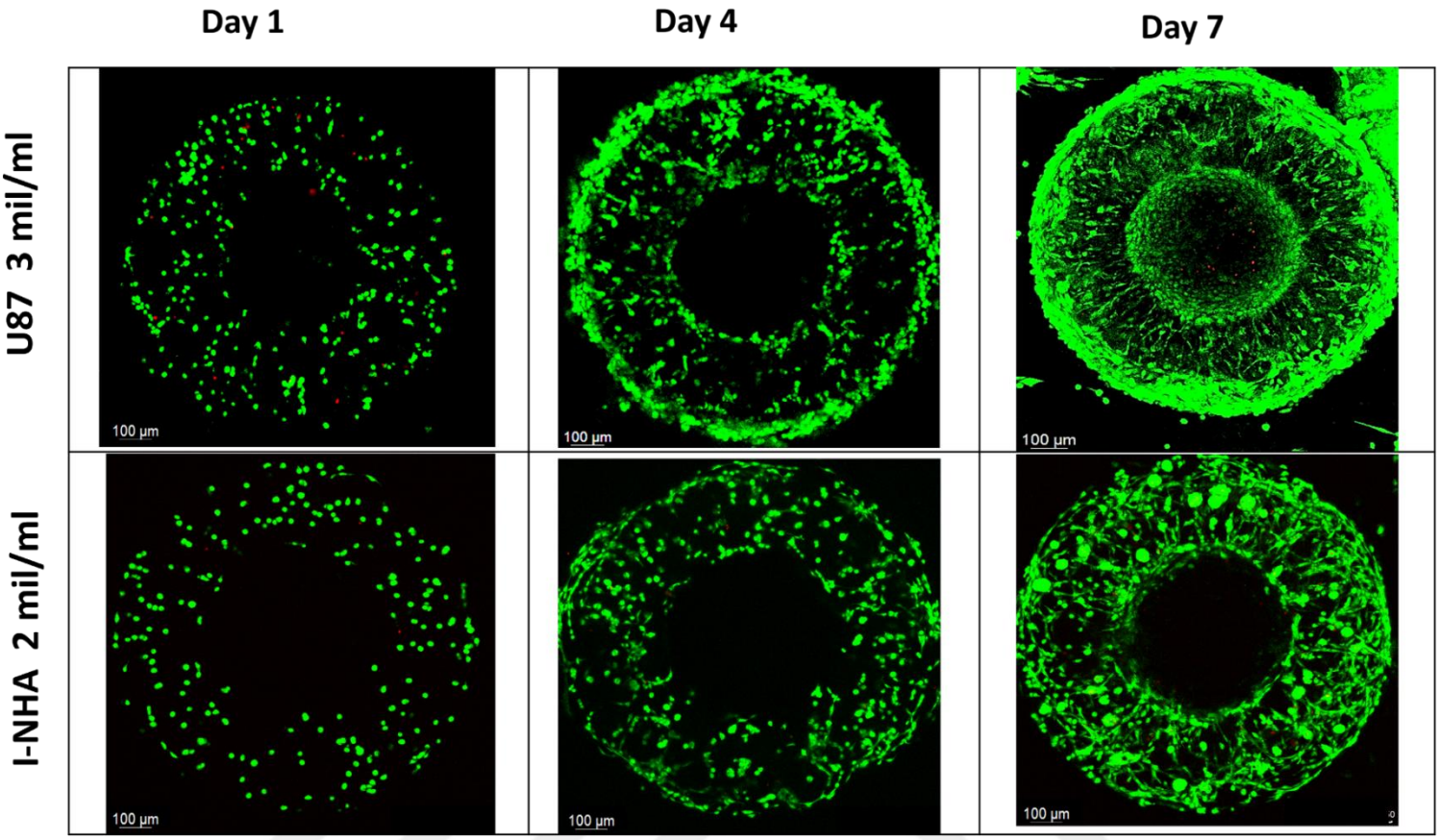

Figure 4.3. The impact of culture duration on the viability of I-NHA and U87 cells within GelMa constructs. *Representative images obtained via Live/Dead assay of U87 and I-NHA cell lines through a one-week period. Living cells are stained with acridine orange (AO), while dead ones with propidium iodide (PI). Scalebar represents 100µm. Both cell types exhibit excellent viabilities within GelMA constructs, only with a minor fraction of cells stained with PI. While U87 cell line migrated outside the doughnuts establishing regions of high cellular density at doughnut edges, I-NHA cells established an interconnected network confined within the boundaries of the doughnut constructs.*

4.2 Development of the Micropatterned Tumor Model

Due to its photocrosslinkable nature and rheological behaviour, GelMA hydrogel is compatible with several biofabrication techniques (Klotz et al., 2016). One of these fabrication methods is photolithrography, which relies on the precise formation of micropatterned tissues by exposing GelMA to UV light through a photomask(Khademhosseini & Langer, 2007). This method offers the advantage of establishing cell-laden constructs of high resolution in a simple and reproducible manner.

This thesis utilized a two-step photolithography method to microfabricate circular tissues containing cells, which were surrounded by pristine GelMA matrices. The approach employed in this study was originally developed by Peela et al. for investigating the migratory behavior of various breast cancer cell lines (Peela et al., 2016). In the present work, this technique was adapted for the establishment of the micropatterned model of the GBM TME. Briefly, this method involves fabricating cell-laden circular constructs by photolithography first, and then filling spaces between them with pristine GelMA.

The rheological assessment of 5%(w/v) GelMA storage modulus in real time **(Figure 3.1(A))** suggests that the stiffness of the hydrogel matrix can be finely adjusted by varying UV exposure times from 10 seconds(~200Pa) to 30 seconds(~1520kPa). The GBM tumors were demonstrated to be stiffer than the surrounding peritumoral brain region. The stiffening phenomena is partly driven by the elevated expression of ECM proteins by GBM tumors, such as tenascin-C, fibronectin, HA and brevican as well as the overexpression of HA-related genes such as CD44 (Khoonkari et al., 2022). To mimic the increased stiffness characteristic of glioma tumors, circular regions containing U87 cells were subjected to a UV exposure duration of 25 seconds(1480Pa). Conversely, the surrounding matrices were crosslinked with UV exposure time of 15 seconds to match the stiffness observed in the peritumoral healthy brain. These values are in accordance with the stiffness values reported by Sohrabi et al. In their recent article, the authors of this article reported that ECM stiffness induces the transition in metabolism of GBM cells towards glycolysis, with softer hydrogels favoring migration (Sohrabi et al., 2023). This study alongside with others demonstrates the importance of mechanical properties of ECM in shaping GBM behavior (Marhuenda et al., 2021;

Wang et al., 2021). Therefore, our microfabricated tumor model is also a valuable tool for the investigation of stiffness role in GBM migration and overall behavior.

Representative confocal images in Figure 4.4 illustrate the temporal evolution of U87 cell line behavior within the 3D model. While initially displaying a round morphology at Day 3, cells adopted more extended morphologies with increasing number of cellular protrusions at Day 5. By Day 7, cells invaded the surrounding matrix. By Day 9 of culture, U87 cells inside doughnuts significantly overgrew filling the whole area of the doughnut constructs.

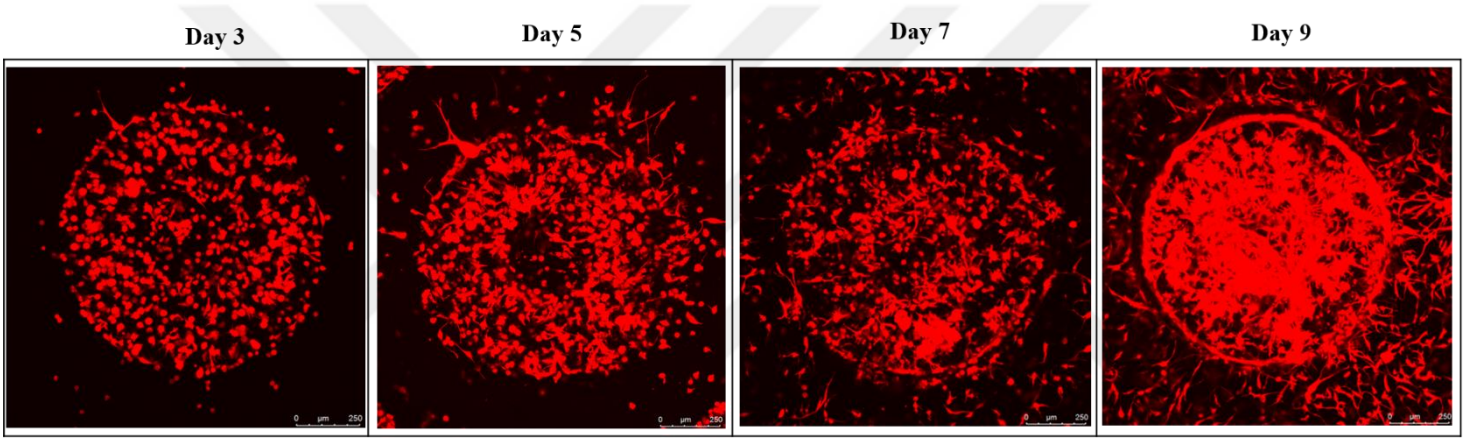

Figure 4.4 The effect of culture duration on U87 cell behavior inside the micropatterned tumor model

Representative confocal images of RFP-U87 cells embedded within GelMA circular constructs and surrounded with pristine GelMa matrices at Days 3,5, 7, and 9 of culture. Scalebar represents 250 μm.

4.3 Visualization of Cytoskeletal Organization of U87 GBM Cells within the Micropatterned Tumor Model

In order to visualize cellular morphology and gain some insight into cell-matrix interactions, F-actin and α-tubulin cytoskeletal organization of cells was examined via immunofluorescence staining. Actin filaments(F-actin), being the key components of the cellular cytoskeleton, were stained with Alexa-Fluor® 488 conjugated phalloidin.

On the other hand, α-tubulin was stained using a two-step immunofluorescence staining approach. First, the cells were incubated with a monoclonal mouse anti-α-tubulin antibody, which specifically binds to α-tubulin protein. After washing off any unbound primary antibody, the cells were then incubated with an anti-mouse secondary antibody conjugated to Alexa-Fluor® 555, emitting a red fluorescence upon excitation. Subsequently, stained samples were incubated with DAPI to visualize cells' nuclei and imaged with a confocal microscope at 10x magnification.

Representative fluorescent images of both cell-embedded circular constructs and their surrounding matrices are presented in **Figure 4.5.** Upon visual examination of the immunofluorescence images, it becomes evident that U87 cells within the circular hydrogel constructs form extensive interconnected networks that span throughout the entire gel volume. Moreover, these images reveal the presence of distinct elongated 3D protrusions exhibited by U87 cells in all regions of the tumor model **(Figure 4.5(A-B))**. Another noteworthy observation is that cells migrating outside the circular constructs established connections with those cells migrating away from adjacent circular constructs **(Figure 4.5(D)).**

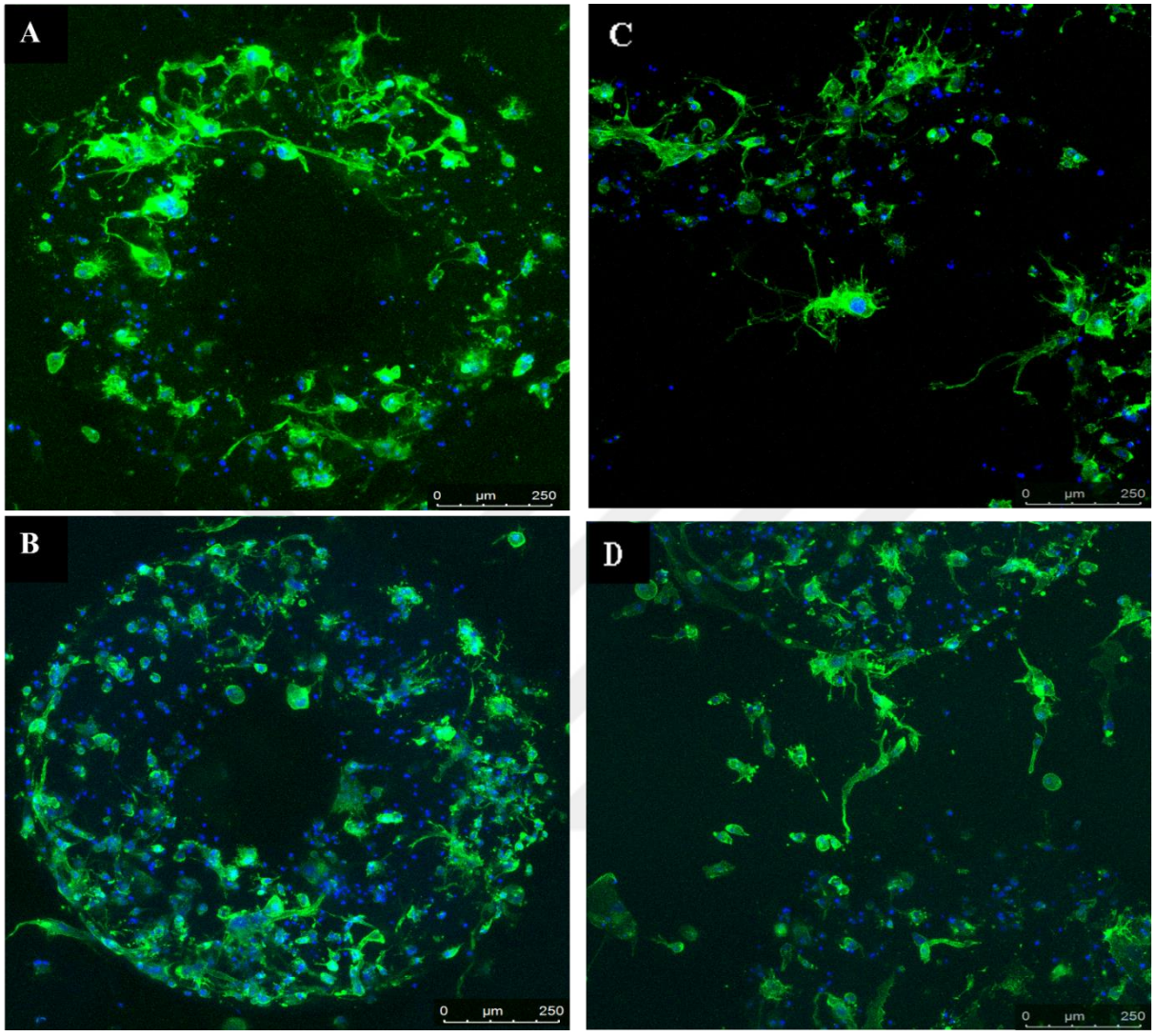

Figure 4.5 Morphological assessment of U87 within the micropatterned tumor model via phalloidin staining *Cytoskeletal organization of cells embedded within GelMA circular constructs and surrounding matrix was visualized by F-actin (green) and Hoechst (blue) staining on Day 5 of culture. Z-stack immunofluorescence images were captured by a confocal microscope at 10X magnification (A-B) Representative images depicting morphology of cells within doughnut hydrogel constructs (C-D) Representative images showing morphology of cells in the surrounding matrices. Scalebar represents 250 µm.*

The immunostaining images of α-tubulin, a protein involved in microtubule formation and cell division, show that U87 cells withing the GelMA hydrogel regions have an increased microtubule density and enhanced bundling of microtubules. This points out that cells within hydrogel constructs have a high proliferative capacity (**Figure 4.6).**

In order to gain a better understanding of the role of matrix stiffness on cellular morphology, phalloidin staining was also performed for hydrogels crosslinked at two different UV exposure times: 10 and 40 seconds. Representative captions are presented in **Figure 4.7.** Thorough visual examination of these images indicates that U87 cells cultured within hydrogels of lower stiffness values exhibit a predominantly rounded morphology. In contrast, cells embedded in hydrogels of higher stiffness (achieved through 40 seconds of UV exposure time) demonstrate an increased presence of actin protrusions and establish interconnected cellular networks.

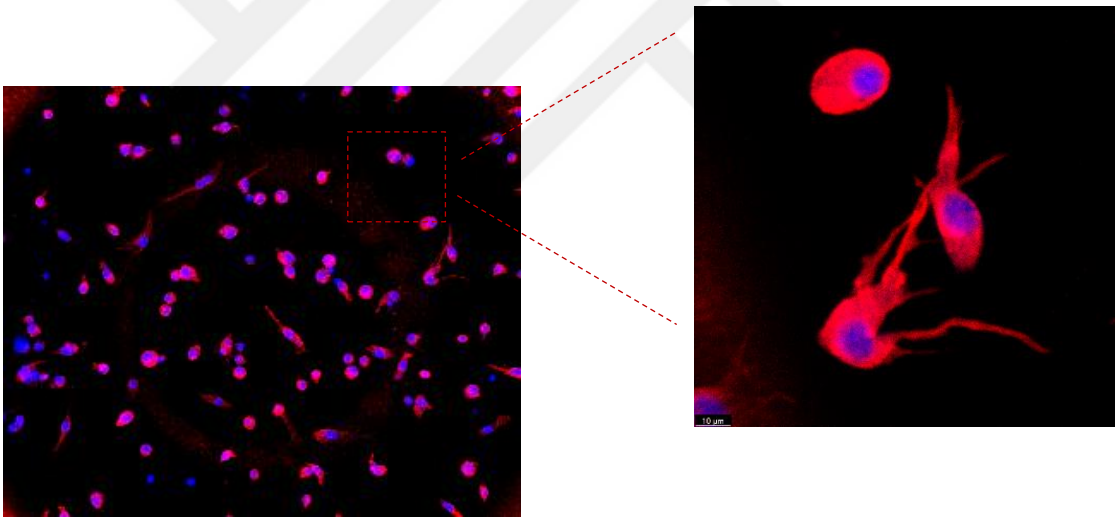

Figure 4.6 Morphological assessment of U87 within the micropatterned tumor model via α-tubulin staining *Immunofluorescence images of α-tubulin (red) and Hoechst (blue) stained GelMA-encapsulated U87 cells on Day 3 of culture. Z-stack immunofluorescence images were captured by a confocal microscope at 10X magnification. Scalebar signifies 10μm.*

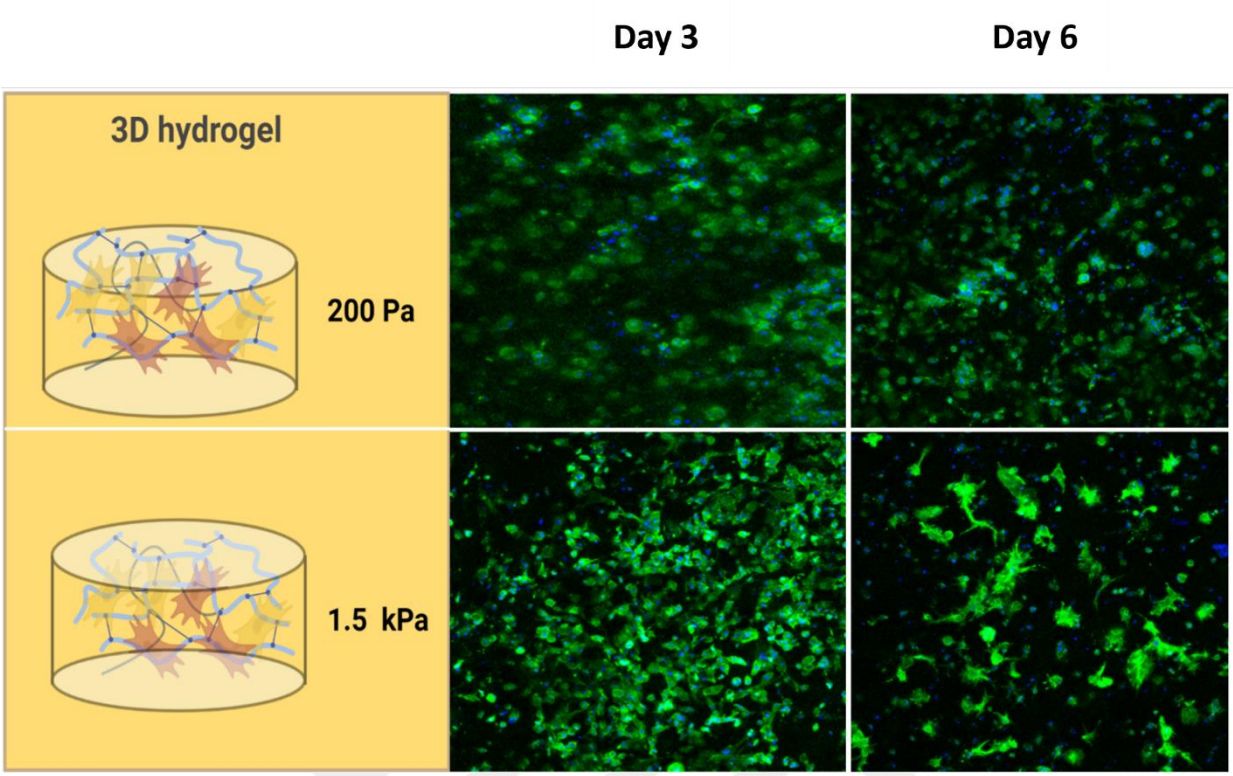

Figure 4.7 Cytoskeletal organization of cells embedded within GelMA circular constructs of varying stiffness values*. The morphology of cells was visualized by F-actin (green) and DAPI (blue) staining on Day 5 of culture. Z-stack immunofluorescence images were captured by a confocal microscope at 10X magnification. Cells within GelMA matrices at 1.5 kPa stiffness exhibit a more elongated morphology compared to those in 200 Pa matrices.*

4.4 Establishment of 3D Micropatterned Co-culture Models of Glioma-Astrocyte Interactions

Establishing a co-culture system of human astrocytes and glioma cells within 3D GelMA constructs involves careful adjustment of experimental parameters, including the co-culture ratio and cell medium composition. I-NHA and U87 cells were both cultured successfully using DMEM high glucose; therefore, a shared medium was employed for co-culture experiments involving these cell types.

In co-culture studies, optimizing the ratio of different cell types is essential for accurately simulating the in vivo environment and facilitating optimal cell interactions. Distinct cell types exhibit varying growth rates, which necessitates careful consideration to prevent any one cell type from dominating the culture, potentially leading to skewed results.

In our study, the determination of cell seeding densities for the co-culture system was informed by MTT viability assay results. The concentration of astrocytes was fixed at 2mil/ml, as this density yielded the most optimal viability for I-NHA cells. However, given that U87 cells proliferate more rapidly than astrocytes, we initially used a lower concentration of 1mil/ml for U87 cells**(Figure 4.8).** This initial setup led to a scenario where astrocytes became dominant within the culture. This dominance resulted in significant growth and migration of I-NHA cells, while the U87 cells exhibited limited migration and predominantly formed aggregates inside the hydrogel constructs by Day 9 of culture in both co-culture configurations. Considering that our study primarily focuses on the migration of U87 cells, we subsequently increased their concentration to 3mil/ml, maintaining the astrocyte concentration constant at 2mil/ml. This adjustment aimed to balance the culture and observe the desired cell interactions, particularly focusing on the migratory behavior of U87 cells in the co-culture system.

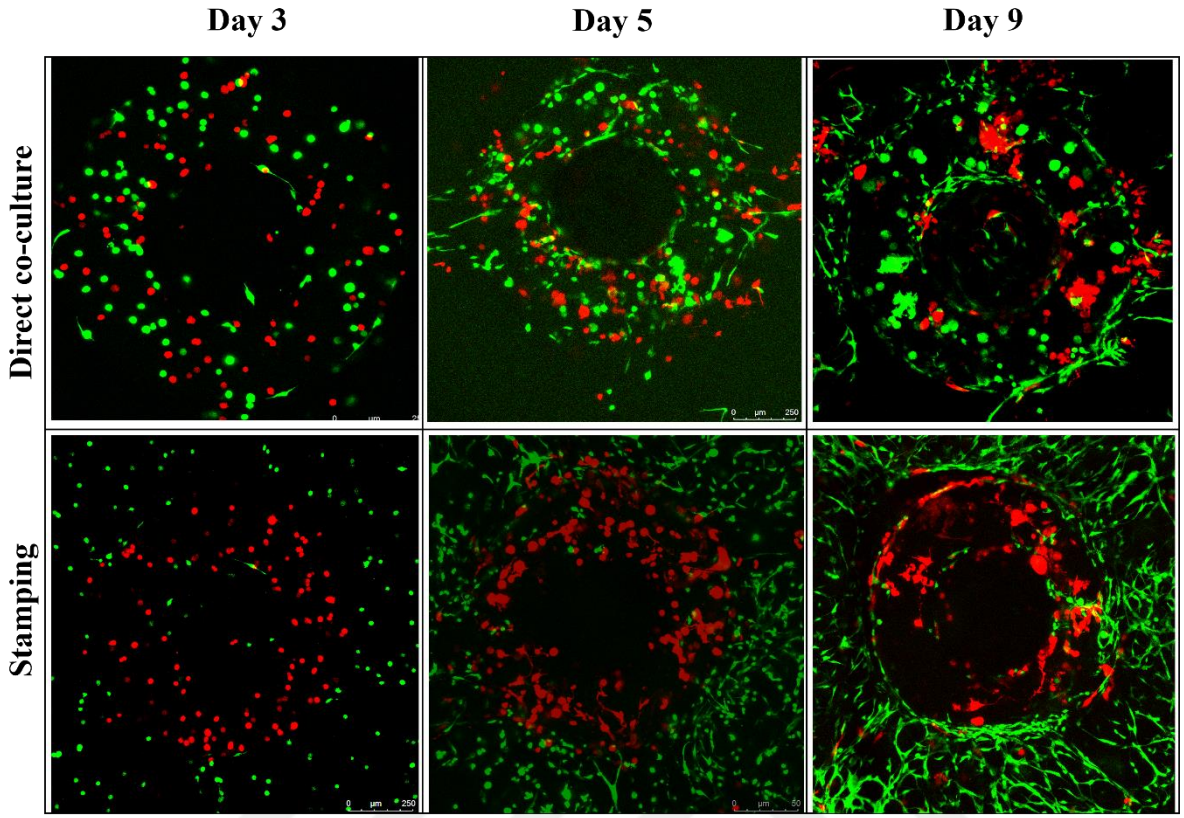

Figure 4.8 Comparative dynamics of two U87-NHA 3D co-culture configurations with 2mil/ml I-NHA and 1mil/ml U87 cell densities. *Representative time-lapse confocal images of two setups of the U87-NHA 3D co-culture system over a 9-day period (Days 3, 5, 9). In both co-culture configurations, the I-NHA cells demonstrated notable growth and migration, whereas the U87 cells showed minimal migration, primarily forming aggregates within the hydrogel constructs by the ninth day of culture. The scalebar represents 250μm.*

The two-step photolithography microfabrication technique described in Section 3.3 granted flexibility in forming two different configurations of astrocyte-glioma co-culture system. The first configuration entailed the direct co-culture of I-NHA and U87 cells inside doughnut constructs, which were surrounded by a matrix of pristine GelMA. This configuration mimics the presence of TAAs in the tumor mass of GBM, therefore it is more suitable for investigating the role of direct astrocyte-glioma interactions in glioma migration and invasiveness. On the other hand, in the second configuration, called "stamping", U87-laden hydrogel doughnuts were surrounded with the astrocyte-dispersed GelMA matrix. This co-culture setup is intended to replicate the conditions in the peritumoral area, where astrocytes are known to be abundant and contribute to the formation of a peritumoral glial scar (Henrik Heiland et al., 2019; Zhang et al., 2023). It was interesting to observe if the co-culture configuration affects the behavior and interaction dynamics of two cell types. For this purpose, two co-culture setups were established from GFP-tagged I-NHA and RFP-tagged U87 and visualized with confocal microscope on Days 3,5, 7, and 9 of culture.

A careful examination of images**(Figure 4.9)** reveals distinctive behavior of U87 cells depending on whether they were cultured in direct proximity to or were surrounded by I-NHAs. In the direct co-culture scenario, U87 cells exhibited robust proliferation and extensive invasion of the surrounding GelMA matrix over a 9-day period. Migratory U87 cells at the interface of doughnuts, and those that infiltrated the surrounding matrix, adopted a spindle like morphology-characteristic of invasive cancer cells with mesenchymal phenotype (Yang et al., 2020)**.** U87 cells that remained inside the doughnuts formed spherical agglomerates that resembled spheroids, with some U87 cells also exhibiting a spindle-like morphology.

In the "stamping" configuration, U87 inside doughnuts also proliferated; however, their growth was confined to doughnut constructs. By Day 5 of the culture, astrocytes, which were homogeneously distributed within the GelMA matrix at Day 3, gradually clustered at the interface with tumor microspheres. By Day 7 of the co-culture, astrocytes had established an extensive network, sequestering U87 cells within the doughnuts. This astrocytic network may contribute to the confinement of U87 cells within the doughnuts, thereby limiting the migratory potential of glioma cells. By Day 9 of culture, confined U87 cells had established many agglomerates resembling tumor spheroids throughout the whole hydrogel construct.

To examine the consistency of U87 cells' invasive behavior in two distinct co-culture setups, we quantitatively assessed their migration capacity. This involved calculating and comparing the areas covered by the migrated cells at various culture intervals (Day 3, Day 5, Day 7, and Day 9) between two co-culture configurations. No significant difference in the number of migrated cells was noted between the two co-culture setups on Day 3**(Figure 4.11(A)).** However, from Day 5, a marked increase in the migratory capacity of U87 cells was observed in the direct co-culture configuration, which soared from an initial 0.83% to 14.32% by Day 9, indicating a nearly 17-fold increase ($p<0.0001$) **(Figure 4.11(B))**. In contrast, U87 cells in the stamping configuration displayed no significant migration throughout the culture period, with the migratory capacity increasing from an initial 0.42% to only 0.67% by Day 9. Consequently, a pronounced divergence in the migratory capacities of U87 cells between the two co-culture configurations became evident from Day 5 and remained consistent for Day 7 and Day 9($p<0,0001$). This data corroborates our observations that U87 cell migration is inhibited in the stamping co-culture setup.

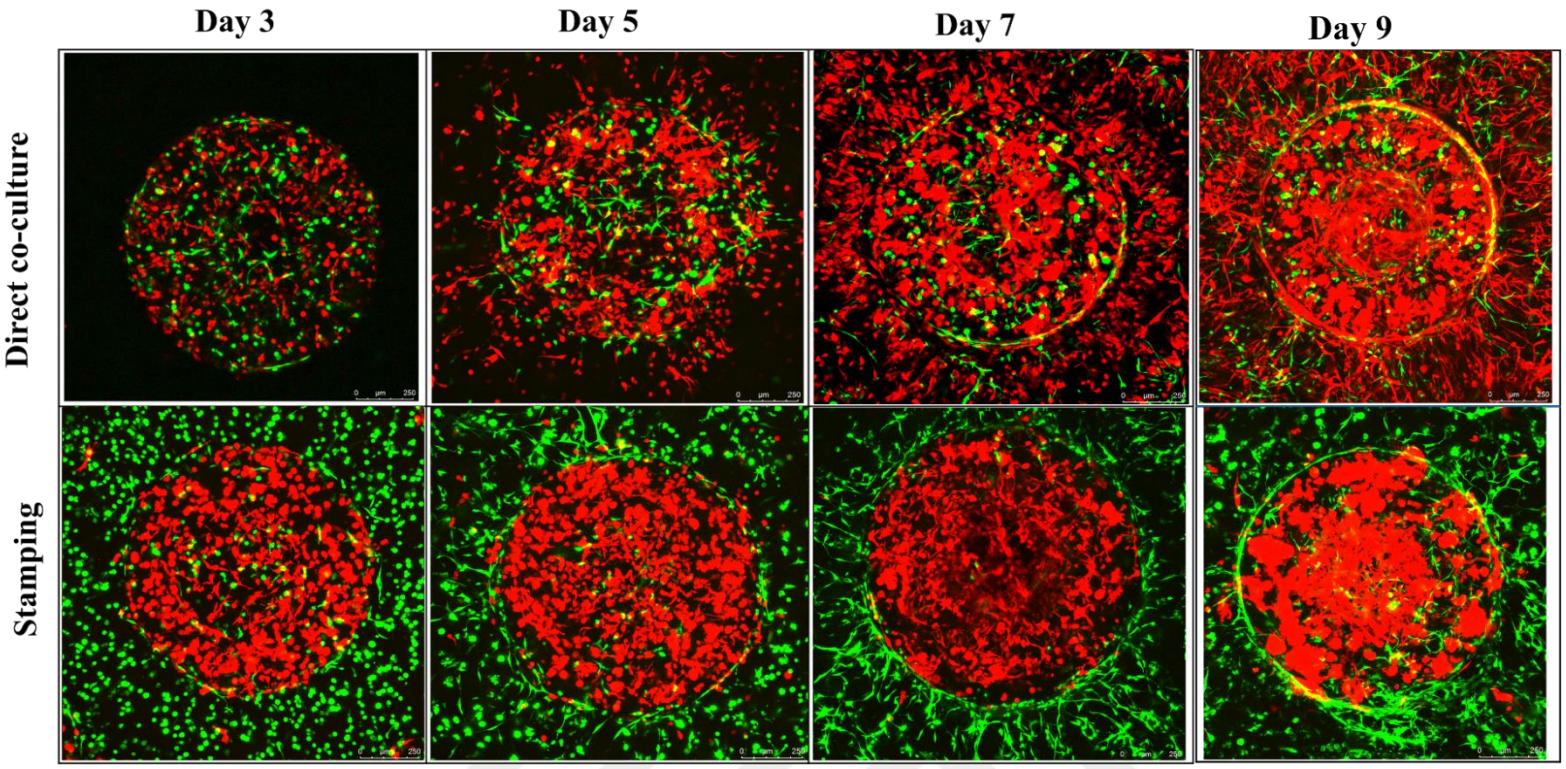

Figure 4.9 Comparative dynamics of two U87-NHA 3D co-culture configurations with 2mil/ml I-NHA and 3mil/ml U87 cell densities. *Representative time-lapse confocal images of two configurations of the U87-NHA 3D co-culture system over a 9-day period (Days 3, 5, 7,9). In the direct co-culture configuration, the RFP-U87 cells displayed a notable migratory capacity, extensively invading the surrounding GelMA matrix by Day 9 of culture. In contrast, within the stamping configuration, U87 cells exhibited limited migration, being confined to doughnut constructs due to the surrounding network of astrocytes. Both co-culture systems consist of 3 mil/mL RFP-tagged U87 cells and 2 mil/mL GFP-tagged NHI cells*. The scale bars in the images represent 250 µm.

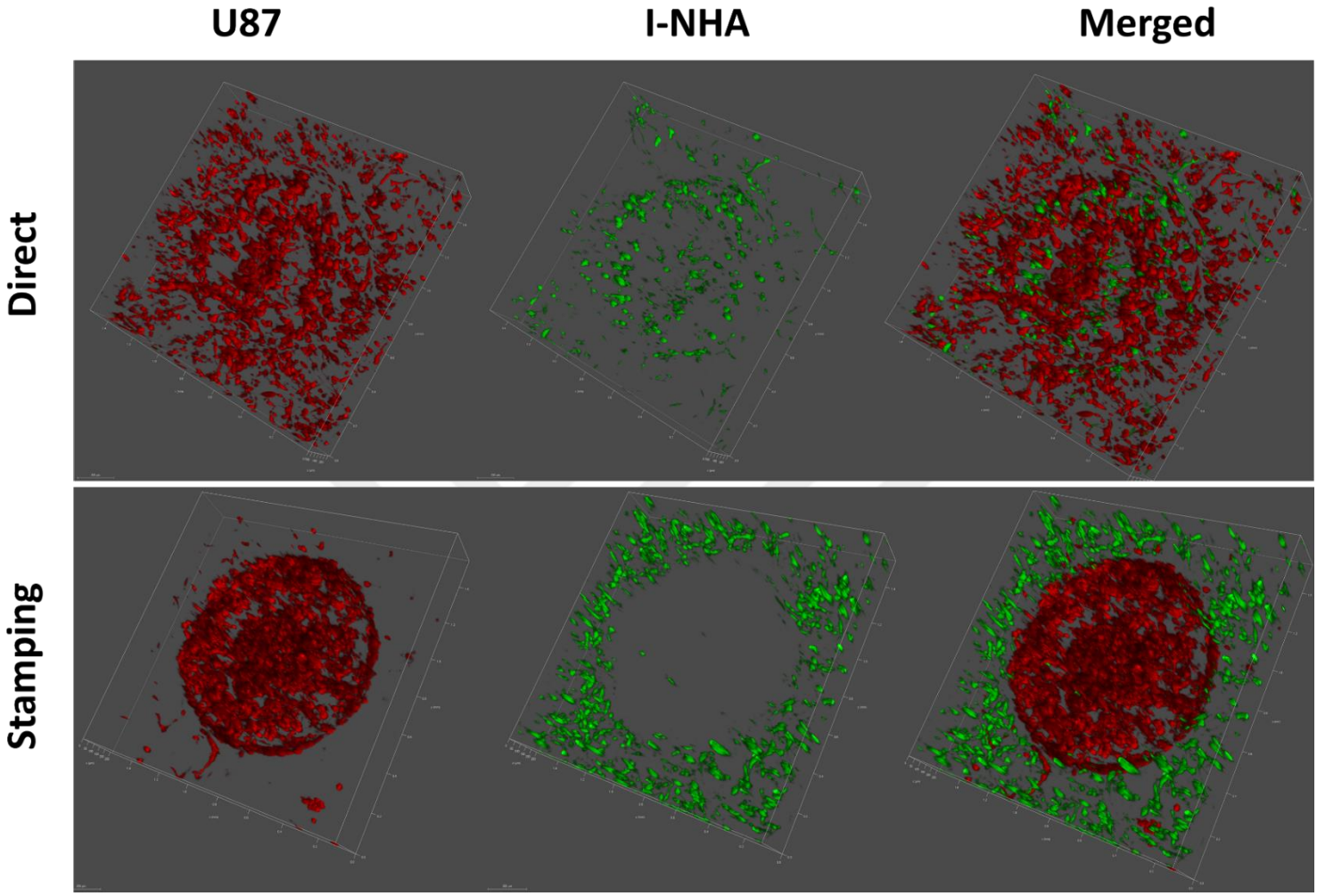

Figure 4.10 3D projections of representative images of two co-culture configurations at Day 7 of culture, demonstrating an extensive migration of RFP-U87 GBM cells throughout the whole hydrogel thickness of 250 µm*. Both co-culture systems consist of 3 mil/mL RFP-tagged U87 cells and 2 mil/mL GFP-tagged NHI cells. The scale bars in the images represent 200 µm.*

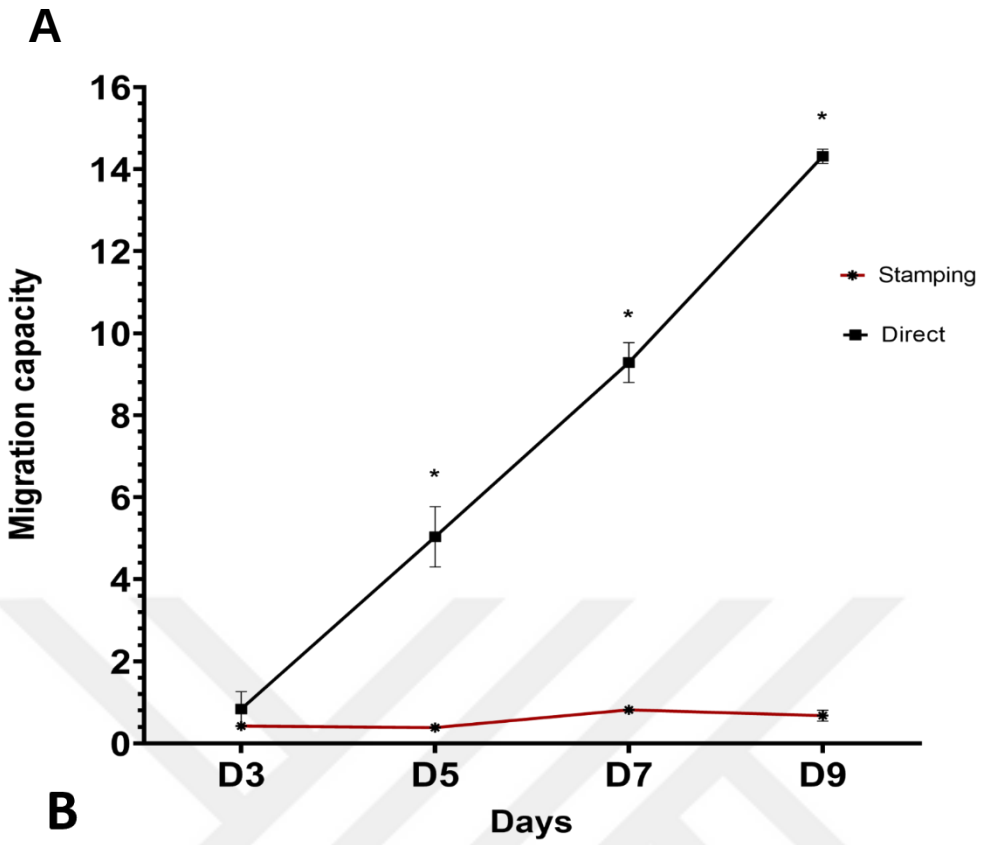
A
Migration capacity
16
14
12
10
8
6
4
2
0
D3
D5
D7
D9
Days
Stamping
Direct
*
*
*
*

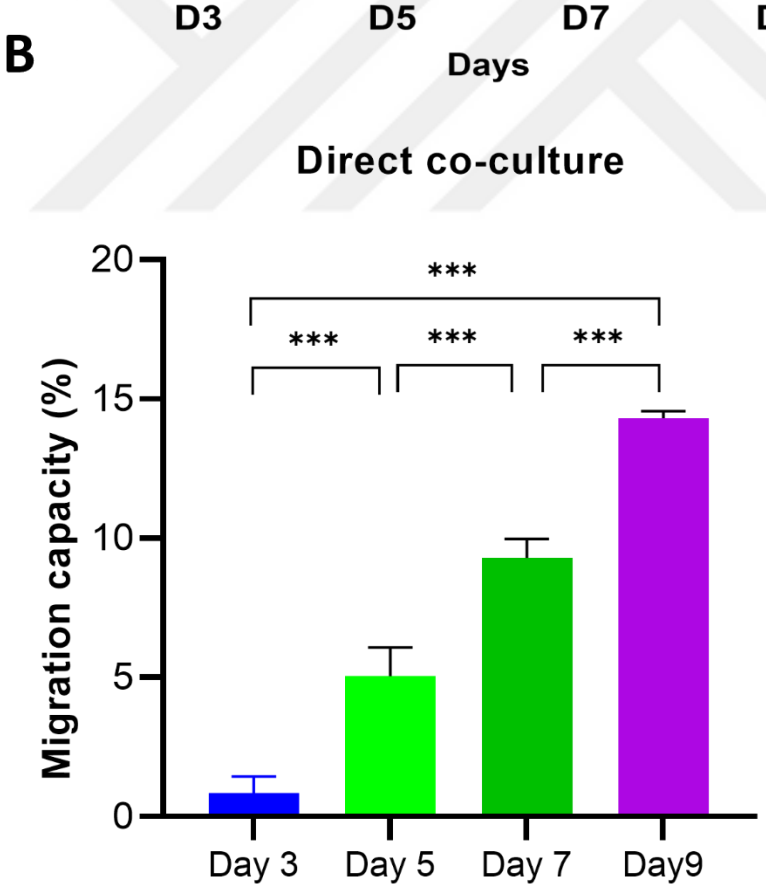
B
Direct co-culture
Migration capacity (%)
20
15
10
5
0
***
***
***
***
Day 3
Day 5
Day 7
Day9

Figure 4.11 Quantitative assessment of the co-culture configuration type on U87 GBM cell line migration capacity. *Migration capacity provides the percentage of the total number of migrated U87 cells with respect to the total area of the frame(1024x1024). Data are presented as the mean ± standard error (N=2).* ***A)*** *A statistically significant increase in migration was observed in the direct co-culture configuration compared to the stamping from Day 5 onwards ($p<0.0001$).* ***B)*** *The migration capacity in the direct configuration showed a consistent upward trend throughout the entire 9-day observation period ($p<0.0001$).*

The observed difference in U87 migratory capacity depending on the astrocyte localization in two co-culture configurations could be explained by different potential reasons. Firstly, the extensive invasiveness of U87 co-cultured in direct contact with I-NHA can be attributed to supportive role of astrocytes in GBM migration. There have been several 3D studies demonstrating the enhanced invasiveness and migratory capacity of GBM cells in the presence of I-NHA cells. For example, Herrera Perez et al. found that astrocytes promote the migratory capacity of patient-derived GBM cells inside collagen-HA hydrogels in a STAT3-dependent way (Herrera-Perez et al., 2018). Furthermore, the presence of astrocytes in GBM-astrocyte spheroids was shown to upregulate the stemness and invasiveness of GBM cells (Nakod et al., 2021). It has also been established that astrocytes augment the migration and treatment resistance of GBM cells through direct cellular communication via gap junctions and tunneling nanotubes (Guan et al., 2018). Notably, reactive astrocytes have been implicated in mediating mitochondrial transfer through tunneling nanotubes, thereby safeguarding GBM cells against chemotherapy in HA-gelatin-based hydrogel models (Civita et al., 2019). The enhanced migratory potential of GBM cells in our model could potentially be attributed to the formation of direct interactions, an aspect, absent in the “stamping” configuration. However, additional experiments are required to conclusively ascertain the specific role of astrocytes in U87 migration within our model.

When it comes to the stamping configuration, the inhibited migration of U87 cells and their confinement to spherical agglomerates by surrounding astrocytes could be explained by the formation of a structure resembling an astrocytic glial scar. The glial scar, primarily formed by reactive astrocytes, microglia, and NG2 glia, is a dense structure that encapsulates brain lesions (Andersen et al., 2021). A key aspect of this

process involves scar-forming astrocytes upregulating CSPGs, which are known to repel regenerating axons in vitro, leading to failed regeneration (Adams & Gallo, 2018). This mechanism suggests that CSPG secretion by reactive astrocytes could hinder the migration of U87 cells from GelMA microspheres in your study, as the presence of CSPGs may impede the formation of actin protrusions, which are crucial for cell migration.

Supporting this hypothesis, recent research has shown that the astrocytic scar can indeed restrict GBM growth and migration (Diep et al., 2023). In a 3D assembloid and mouse xenograft model, it was observed that glutamate released from a GBM-microglia assembloid significantly upregulated the activity of astrocytic MAO-B and the deposition of CSPGs, contributing to the formation of the astrocytic scar. This scar formation was linked to restricted GBM growth. Moreover, when scar formation was inhibited, there was an increase in drug penetration into the GBM assembloid, along with a reduction in GBM confinement.

4.5 The Impact of U87 Cells on Astrocyte Reactivity

The phase-contrast images captured at 10x magnification offer enhanced resolution, facilitating a detailed examination of the astrocytic network closely encircling the U87 microspheres **(Figure 3.4).** This network is composed of star-shaped astrocytes with enlarged cell bodies, which form extensive connections through their branches. In contrast, the astrocytes surrounding doughnuts lacking U87 cells exhibit a different morphology. While these astrocytes do form networks with some connections, their cell bodies are not enlarged, and the extent of their branching is markedly less compared to those around the U87 microspheres.

The formation of an extensive network of astrocytes surrounding U87 microspheres in the stamping co-culture configuration can be attributed to the reactive phenotype of astrocytes. Astrocytes were reported to transform into their reactive counterparts when they contact tumor cells by several studies(Campbell et al., 2020; Guan et al., 2018). Activated astrocytes not only secrete a substantial amount of growth factors, cytokines and other soluble factors but can also participate in the formation of a

physical barrier termed a “glial scar”, potentially isolating the GBM tumor from the surrounding brain tissue (Sofroniew & Vinters, 2010). Reactive astrocytes exhibit distinctive features, including the hypertrophy of cellular bodies and an overexpression of GFAP(Haim et al., 2015).

Therefore, to check the reactivity of astrocytes and to better visualize their morphology in the presence of U87 doughnuts, the GFAP filaments of astrocytes were visualized by using immunocytochemical staining. The co-culture GFAP images were compared against the immunofluorescence images obtained from astrocytes surrounding empty doughnuts with no dispersed U87 cells. In the presence of U87 cells, astrocytes established interconnected branches of GFAP filaments spanning the whole space between U87 doughnuts. In contrast, astrocytes surrounding empty doughnuts exhibited predominantly round morphology, with several cells having extended spindle-like morphologies. The observed difference in astrocyte phenotype indicates the potential existence of a dynamic and bilateral communication between GBM cells and surrounding astrocytes in our platform.

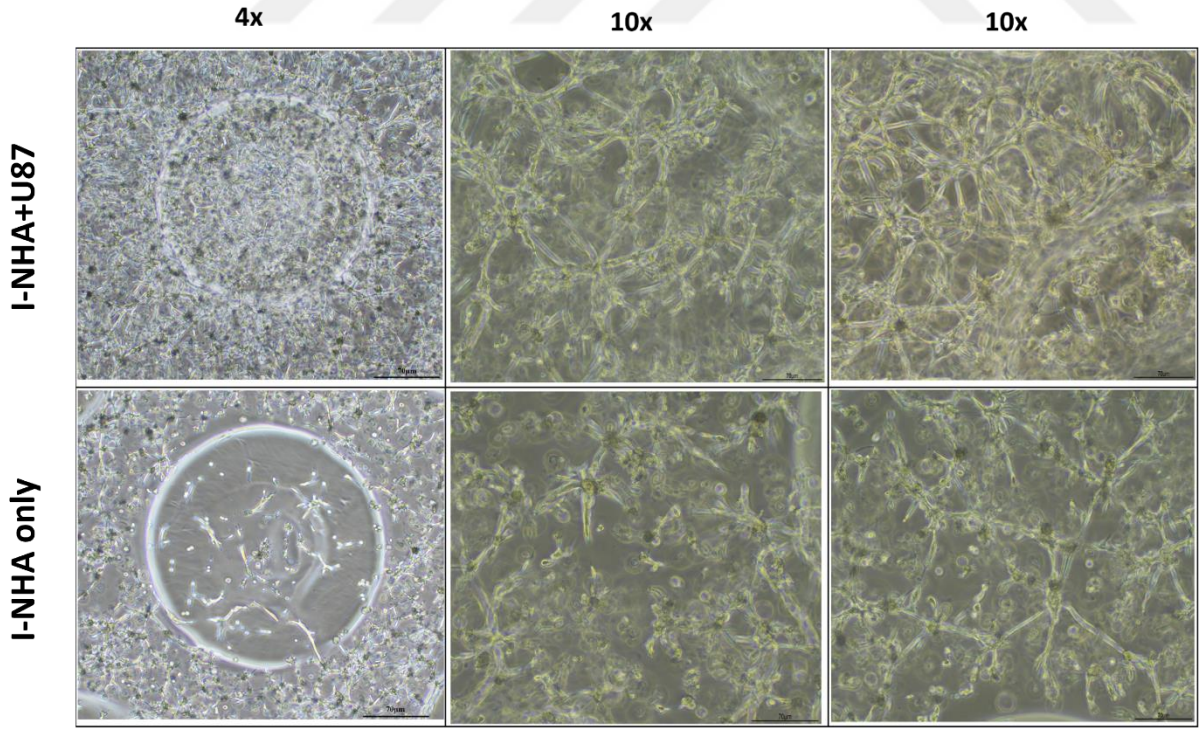

Figure 4.12 Astrocytic network development around U87 tumor microspheres.
Representative phase-contrast images at 4x and 10x magnification displaying a stark contrast between extensive, interconnected astrocytic networks around U87 tumor microspheres, compared to astrocytes with fewer branches in environments without U87 tumor cells. Scalebar represents 70µm.

However, experimental group in our setup contained a larger overall concentration (5mil/ml) of cells when compared to the control (2mil/ml), which introduces a variable that might independently affect astrocyte behavior. The increase in GFAP expression in astrocytes could be a response to the higher cell concentration in the experimental group, rather than a specific response to the identity of U87 glioblastoma cells. To exclude this possibility, additional experiments with another cell type inside the hydrogel doughnuts could be performed. Incorporating a control group with astrocytes alone, at comparable cell concentrations, would help determine if the changes in astrocyte morphology and network formation are indeed due to the presence of U87 cells or are a result of the cell concentration differences.

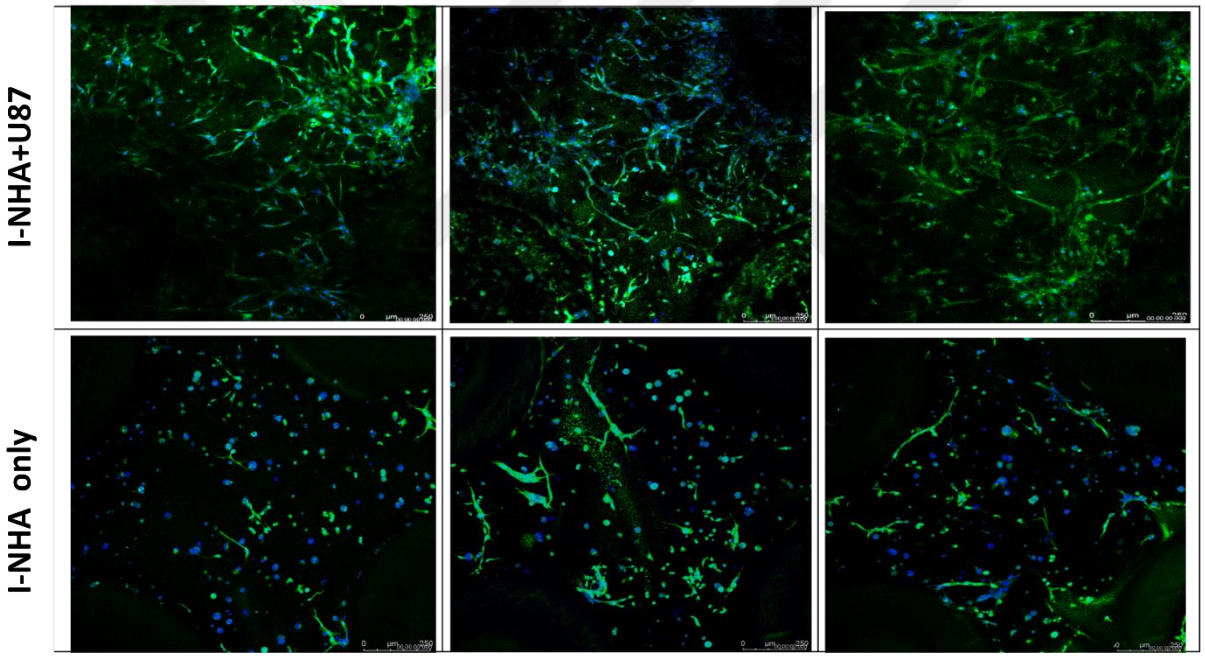

Figure 4.13 The immunocytochemical analysis of astrocyte reactivity around U87 microspheres
The reactive status of astrocytes surrounding U87 GBM microspheres was checked by performing immunocytochemical staining (green) against GFAP intermediate filaments at Day 5 of culture. Cell nuclei were counterstained with Hoechst (blue). The representative images demonstrate the formation of an extensive network of astrocytes in the presence of U87 cells in contrast to the control group containing no cells inside GelMA microspheres. Z-stack immunofluorescence images were captured by a confocal microscope at 10X magnification. Scalebar represents 250µm.

4.6 Gene Expression Analysis of U87 Cells inside the Micropatterned Model of the GBM TME

The influence of 3D culture conditions on gene expression profiles of cells is an active area of investigation. There is a large body of research that has substantiated that the 3D culture environment exerts a profound influence on the gene expression levels of cells, leading to behaviors that are closer to those observed in vivo (Abbas et al., 2023; Imamura et al., 2015; Takahashi et al., 2015; Tekin et al., 2018). In this thesis we attempted to assess how culturing U87 cells inside our micropatterned platform affects the expression of genes associated with GBM invasiveness and malignancy. We performed qPCR in three different set-ups, each aiming to unravel the effects of various microenvironmental factors of our system on the behavior of U87 GBM cells.

1) 3D and 2D Culture Comparison:

In the first set-up, we compared the gene expression profiles of U87 cells grown inside our micropatterned platform versus those grown in 2D plastic culture flasks. This setup was designed to deepen our understanding of how 3D culture conditions within GelMA hydrogel influence GBM cell malignancy and invasion.

2) Impact of Astrocyte Co-culture in 3D:

Our second setup focused on the role of co-culturing astrocytes with U87 cells within the 3D platform. Here, the aim was to explore how the presence of astrocytes affects GBM invasiveness, recognizing the importance of intercellular interactions in tumor progression.

3) Influence of Co-Culture Configuration on Gene Expression:

Finally, building on the observations from Section 3.3 of differential migration behaviors in U87 cells based on co-culture configurations with astrocytes, we aimed to determine if these co-culture arrangements modulate the expression of selected genes of interest. This aspect of the study emphasized the significance of the spatial arrangement of tumor and stromal cells in influencing gene expression patterns of the co-culture system.

4.6.1 Gene Expression Analysis of the 3D Culture Effect on U87 GBM Cells

Given the primary focus of this thesis on investigating the migratory behavior of GBM cells, the gene expression analysis via qRT-PCR was conducted specifically targeting genes associated with GBM invasiveness and EMT, namely MMP-2, MMP-3, MMP-9, MMP-14, VEGF, HIF-1α, TGF-β, CD44, and fibronectin. To evaluate the impact of 3D culture conditions and geometry on the invasiveness of GBM in a quantitative way, mRNA expression levels of these genes were normalized with respect to those of U87 cells grown in 2D (Figure 3.5).

The bar charts of qPCR results (Figure 3.5(A)(C)) distinctly demonstrate a significant upregulation of MMP-2 and MMP-9 expressions within the 3D GelMA hydrogel compared to 2D culture conditions, with P-values of 0.0003 and 0.00146, respectively. Notably, both genes exhibited an approximate two-fold increase in expression levels, indicating a robust response to the 3D culture environment. Furthermore, MMP-14 and MMP-3 **(Figure 3.5(B)(D))** also showed substantial increases in expression under 3D conditions compared to 2D culture, with MMP-14 displaying a three-fold increase (p=0.0002) and MMP-3 showing an even more pronounced 3.5-fold increase (p=0.0008).

MMPs have been implicated in a number of cancer types as important drivers of tumor malignancy, invasion and metastasis (Azevedo Martins et al., 2020; Hidalgo & Eckhardt, 2001). Gelatinases MMP-2 and MMP-9 are increasingly recognized as crucial prognostic markers in the recurrence of gliomas. In addition, their elevated expressions correlate with a high glioma grade (Zhou et al., 2019). These enzymes mediate the degradation of the ECM and are instrumental in promoting angiogenesis, two processes that are key to the invasiveness of glioma cells (Ulasov et al., 2014; Wang et al., 2003). Unlike MMP-2 and MMP-9 which are soluble enzymes, MMP-14 is a membrane-bound protease. But similar to gelatinases, MMP-14 is also critical for glioma proliferation, invasion and angiogenesis, and its overexpression is also associated with a poor outcome and higher glioma grades in glioma patients (Kasten et al., 2020). MMP-14 is also responsible for enhanced glioma migration, as it activates MMP-2 and MMP-9 (Chen et al., 2016). The specific function of MMP-3 in GBM, however, is not as extensively documented as that of MMP-2 and MMP-9. However, several studies

showed the role of MMP-3 in enhanced glioma migration, progression, and aggressiveness (Lee et al., 2010; Pullen et al., 2018; Sun et al., 2014).

A careful examination of qPCR data focusing on the hypoxia-related genes reveals significant changes in the levels of HIF-1α and VEGF in U87 GBM cells cultured within GelMA microspheres. Specifically, there was a nearly two-fold increase ($p=0.0178$) in the expression of HIF-1α and a 1.5-fold increase ($p=0.0143$) in the expression of VEGF. The increase of hypoxia-related factors in our model can be attributed to two potential reasons. Firstly, natural oxygen gradients were shown to exist inside inside low-stiffness GelMA hydrogels (Schmitz et al., 2022). This leads to the presence of hypoxic regions within these 3D hydrogels right from the outset. Second, the GBM cells are characterized by their high metabolic rate, which results in a rapid consumption of oxygen in their environment. Consequently, this intensifies the already existing hypoxic conditions within the GelMA hydrogels. HIF-1α is a transcription factor that accumulates inside the cell as a response to hypoxia leading to the expression of various genes that aid in adaptation to low oxygen environments (Kaur et al., 2005). One of these genes is VEGF, which is a highly cytokine known to promote angiogenesis. The upregulation of these growth factors plays a critical role in GBM, particularly in terms of its influence on tumor growth, treatment resistance and invasiveness(Gauthier et al., 2020; Lo Dico et al., 2018).

When it comes to other EMT-related genes such as TGF-β, CD-44 and FN1, they also experienced a robust upregulation of their expression levels (Figure 3.6). Specifically, the expression of the TGF-β cytokine showed a 1.8-fold increase ($p=0.0002$). The rise in TGF-β is linked to a poorer prognosis in GBM patients, as it can trigger a mesenchymal transformation in GBM cells through the activation of EMT transcriptional factors such as SMAD2 and ZEB1 (Joseph et al., 2014). CD44, a marker associated with the stemness and mesenchymal subtype of GBM (Inoue et al., 2023), exhibited a 1.5-fold increase in expression ($p=0.0024$) in U87 cells grown under 3D culture conditions compared to 2D cultures. Additionally, fibronectin, another crucial EMT marker (Chen et al., 2021), showed a significant 3.3-fold increase ($p<0.0001$) in expression in cells cultured within the GelMA hydrogel.

Taken together, described gene expression changes suggest that U87 GBM cells exhibit a more invasive and malignant phenotype inside 3D GelMA hydrogels when compared to U87 cells grown on traditional 2D culture flasks. The marked upregulation

of MMP-2, MMP-9, MMP-14, and MMP-3 under 3D conditions underscores the influence of the microenvironment in the context of matrix remodeling and invasion, which are the key characteristics of tumor aggressiveness. Additionally, the significant upregulation of EMT-related genes such as TGF-β, CD-44, and FN1 in the 3D environment of GelMA hydrogel further implies a shift towards a mesenchymal, more invasive phenotype in U87 GBM cells. These results support the recent findings of Shah et al., who demonstrated that patient-derived GBM cells grown inside GelMA hydrogels are enriched for the treatment-resistant mesenchymal phenotype when compared to neurosphere culture and cells in 2D (Shah et al., 2021).

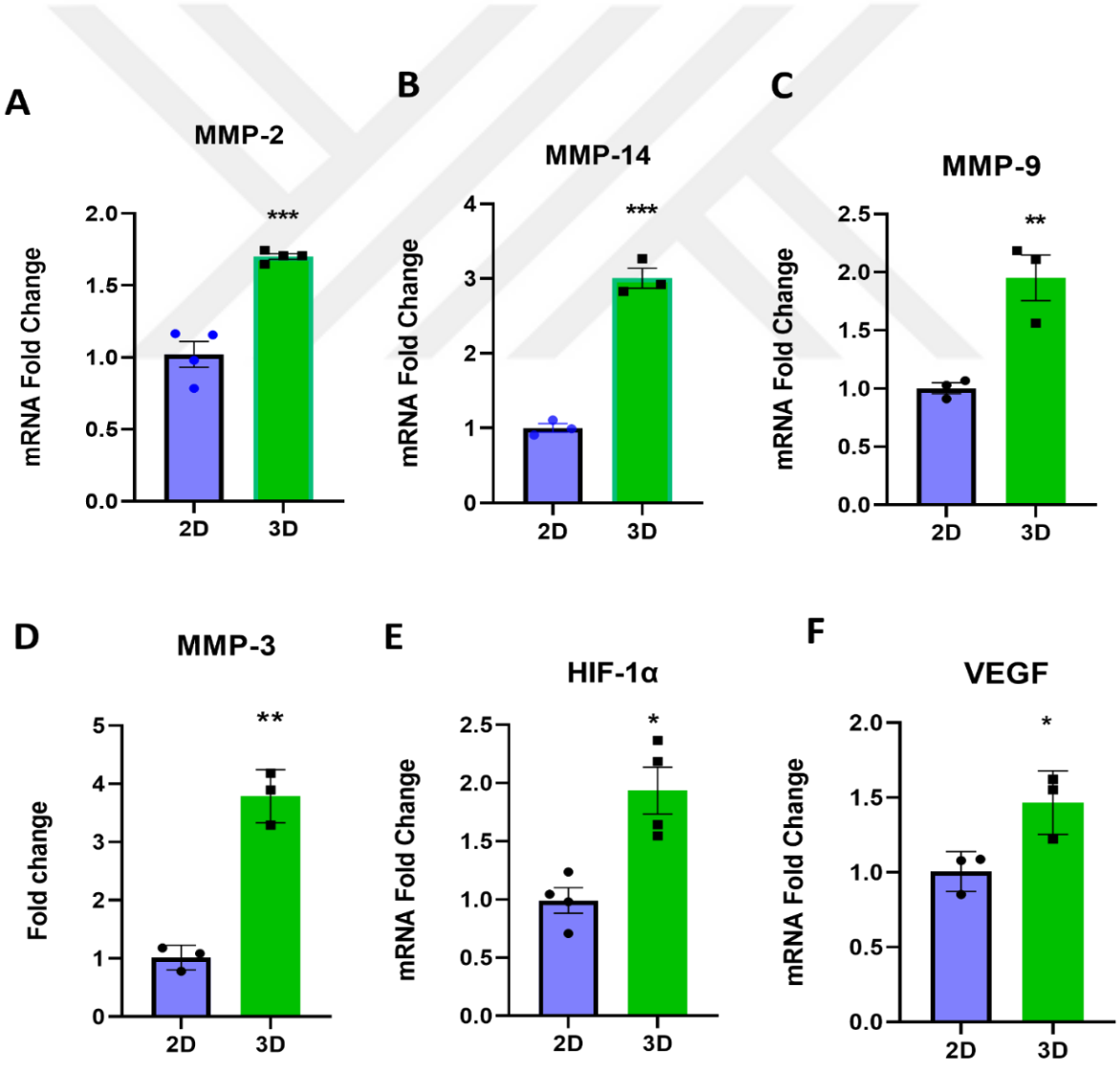

Figure 4.14 The bar charts visually representing the gene expressions of invasion-related MMP enzymes and hypoxia-related factors (VEGF and HIF-1α) as determined by quantitative real-time PCR. *mRNA expression levels were calculated for RNA lysates extracted from gel constructs at Day 4 after encapsulation. Gene expressions of cells grown within GelMA constructs were calculated relative to the ACTB housekeeping gene and normalized to those of cells cultured on traditional 2D plastic plates. The bar charts represent the Mean±SEM of expression values derived from n ≥3 independent experiments, each conducted in triplicate. Statistical significance was assessed using unpaired t-test, denoting (*) for $p < 0.05$, (**) for $p < 0.01$, and (***) $p < 0.001$*

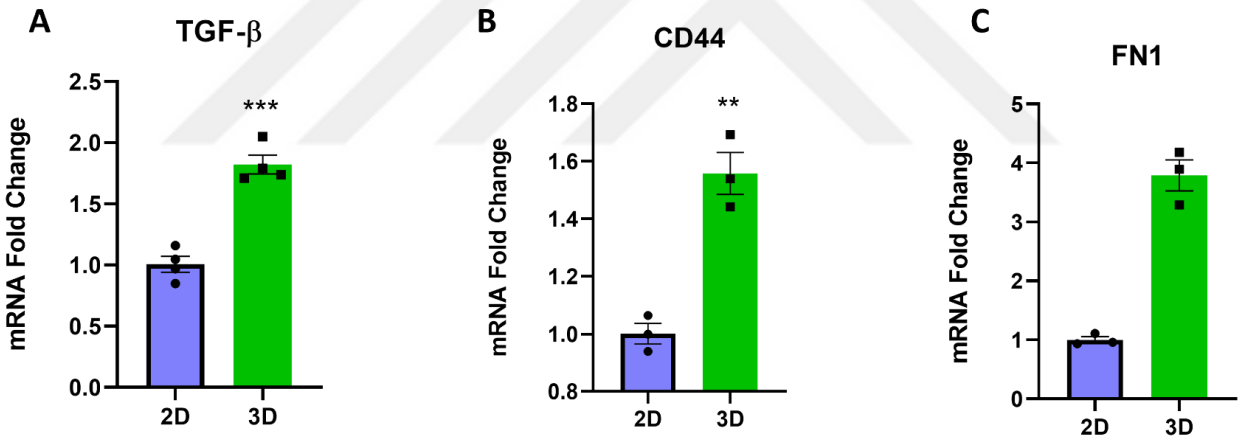

Figure 4.15 The bar charts visually represent the expression profiles of genes related to epithelial-to-mesenchymal transition (EMT) in U87 cell line as determined by quantitative real-time PCR. *mRNA expression levels were calculated for RNA lysates extracted from gel constructs at Day 4 after encapsulation. Gene expressions of cells grown within GelMA constructs were calculated relative to the ACTB housekeeping gene and normalized to those of cells cultured on traditional 2D plastic plates. The bar charts represent the Mean±SEM of expression values derived from n ≥3 independent experiments, each conducted in triplicate. Statistical significance was assessed using unpaired t-test, denoting (*) for $p < 0.05$, (**) for $p < 0.01$, and (***) $p < 0.001$*

4.6.2 Gene Expression Analysis of the I-NHA Co-culture Effect on U87

Despite numerous studies reporting the effect of astrocyte co-culture on the expression of target genes in GBM cells (MMP-2,MMP-9,MMP-14, IL-6,HIF-1α, VEGF)(Li et al., 2010; Loeffler et al., 2005; Zhang et al., 2020), our study did not show any significant impact of astrocytic co-culture on the gene expression profile of our co-culture system. All of the selected genes exhibited non-significant difference in expressions between co-culture experimental group and individual cell types (U87 and I-NHA) cultured together(P>0,05)

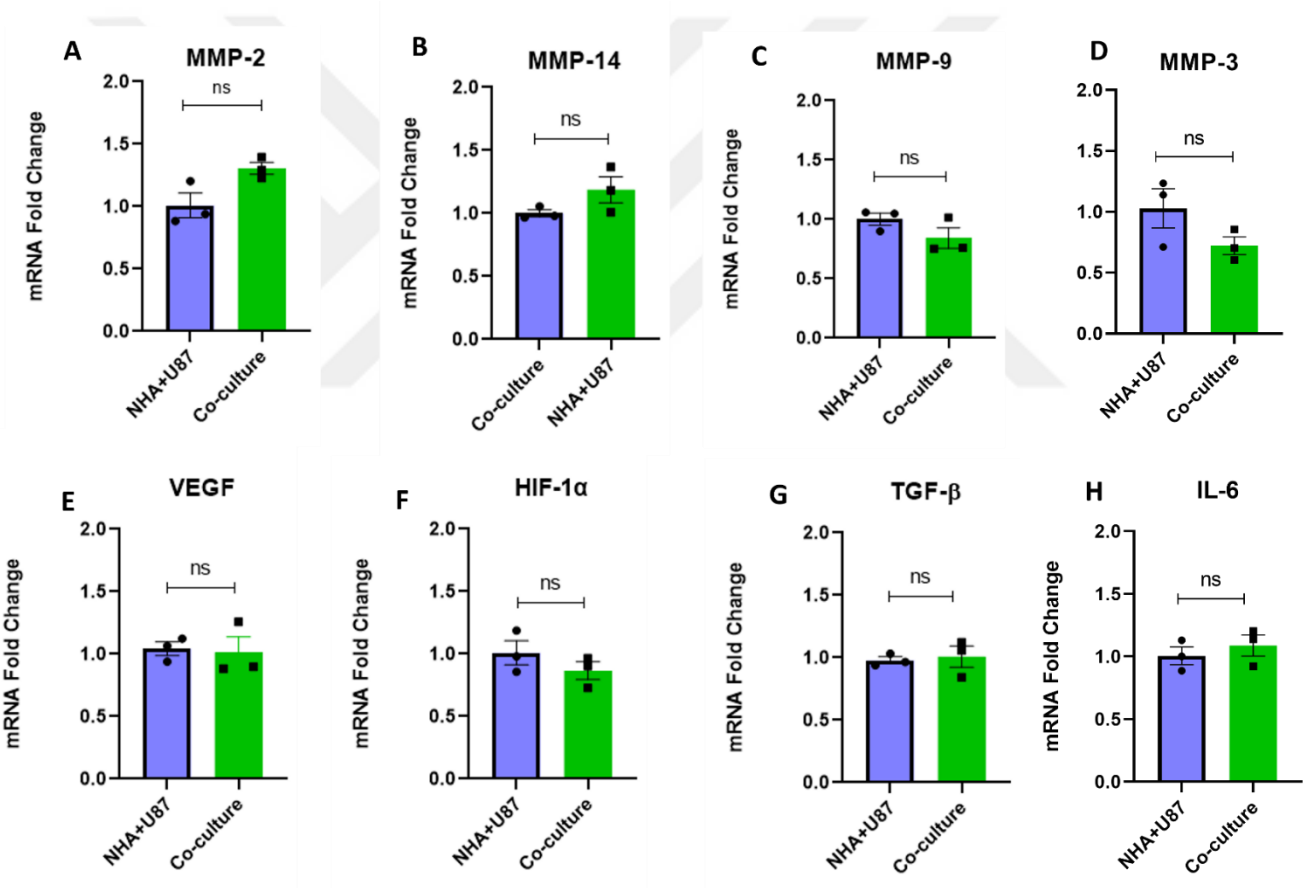

Figure 4.17 The bar charts depict the effect of I-NHA co-culture on the gene expression level of the co-culture system. *RNA expression levels were calculated for RNA lysates extracted from gel constructs at Day 4 after encapsulation. Results of co-culture were normalized to the gene expression of the mixture of I-NHA and U87 grown individually. None of the targeted genes showed a significant difference in expression level between co-cultured cells versus cells grown in monoculture. Statistical significance(N=3-4) was assessed using unpaired t-test, denoting (ns) for p>0,05*

4.6.3 Evaluation of the Co-culture Configuration Effect on the Gene Expression of the Co-culture System

To quantify the distinct behaviors of U87 and I-NHA cell lines in two co-culture setups, we performed a qPCR analysis on mRNA extracted from these systems. An examination of the bar charts in Figure 4.3, which visually depict the gene expression changes, reveals significant differences. In the direct co-culture configuration, where U87 cells were in direct contact with I-NHA cells, there was a notable upregulation in the transcription of MMP-9, MMP-3, MMP-14, and TGF-β genes. Specifically, MMP-9 showed almost a two-fold rise ($p=0.0321$), while MMP-14 and MMP-3 exhibited approximately 1.2 and 1.5-fold increases, respectively ($p=0.0095$ and $p=0.0462$). The observed overexpression of MMPs, including MMP-9, MMP-14, and MMP-3, along with the cytokine TGF-β, is indicative of a more aggressive, invasive phenotype in GBM cells. This finding is in line with the confocal imaging data, which distinctly illustrate the pronounced migratory capacity of U87 cells within the direct 3D co-culture environment with astrocytes. It is important to note, however, that MMP-2, unlike its counterparts, did not exhibit significant variances in expression across the two co-culture configurations.

The contrasting trend was observed for IL-6 cytokine and hypoxia-related factors such as VEGF and HIF-1α. These genes' expressions were upregulated in the stamping configuration. The higher expression of hypoxia-related factors could be explained by the formation of spheroid-resembling agglomerates by U87 cells in the stamping configuration. Being trapped in the surrounding network of astrocytes, U87 were unable to migrate, therefore accumulating inside the doughnut constructs and experiencing hypoxia. As a part of the regulatory response to hypoxia in tumors, U87 cells potentially induced the release of HIF-1α, influencing the angiogenesis through VEGF expression.

Interestingly, the observed overexpression of IL-6 in this setup initially appears counterintuitive, considering its association with the migratory behavior of U87 cells and high MMP protease levels in other studies(Chen et al., 2016; Li et al., 2010). However, the role of IL-6 in GBM is more complex: apart from being a promoter of GBM invasion, IL-6 is an important marker of astrocyte reactivity modulating immune

response to tumor progression (Brandao et al., 2019). Therefore, the elevated IL-6 levels in this setup could reflect the neuroinflammatory response of astrocytes to the tumor environment, possibly contributing to the formation of a peritumoral glial scar and impacting the behavior of the U87 cells.

Nevertheless, the potential explanation for the gene expression patterns of IL-6 as well as other studied genes could be the following. In the stamping co-culture configuration, astrocytes are more dominant when compared to U87 cells: they establish an extensive network of large area, while U87 cells are confined to doughnut structures. Since RNA was extracted directly from the co-cultured cells, containing mixtures from both cell types, the gene expression profile in the stamping configuration likely skewed towards astrocytes, which express IL-6 more abundantly than U87 cells, as indicated by our previous qPCR studies. In contrast, the direct co-culture setup, with a higher predominance of U87 cells, mirrored the gene expression profile of these cells more closely, especially regarding MMP enzymes, which are expressed at higher levels in U87 cells than in I-NHA cells.

If the gene expression profiles are influenced by the most dominant cell type, this can lead to results that are more reflective of the behavior of that particular cell type rather than the interactive effects of co-culturing. For a more accurate investigation of the gene expression changes in U87 cells across the two co-culture setups, it would be beneficial to isolate U87 cells from the hydrogel constructs and sort them using FACS. This approach would minimize the 'noise' from astrocytic RNA, providing a clearer view of the specific gene expression alterations in U87 cells due to the different co-culture conditions with I-NHA cells.

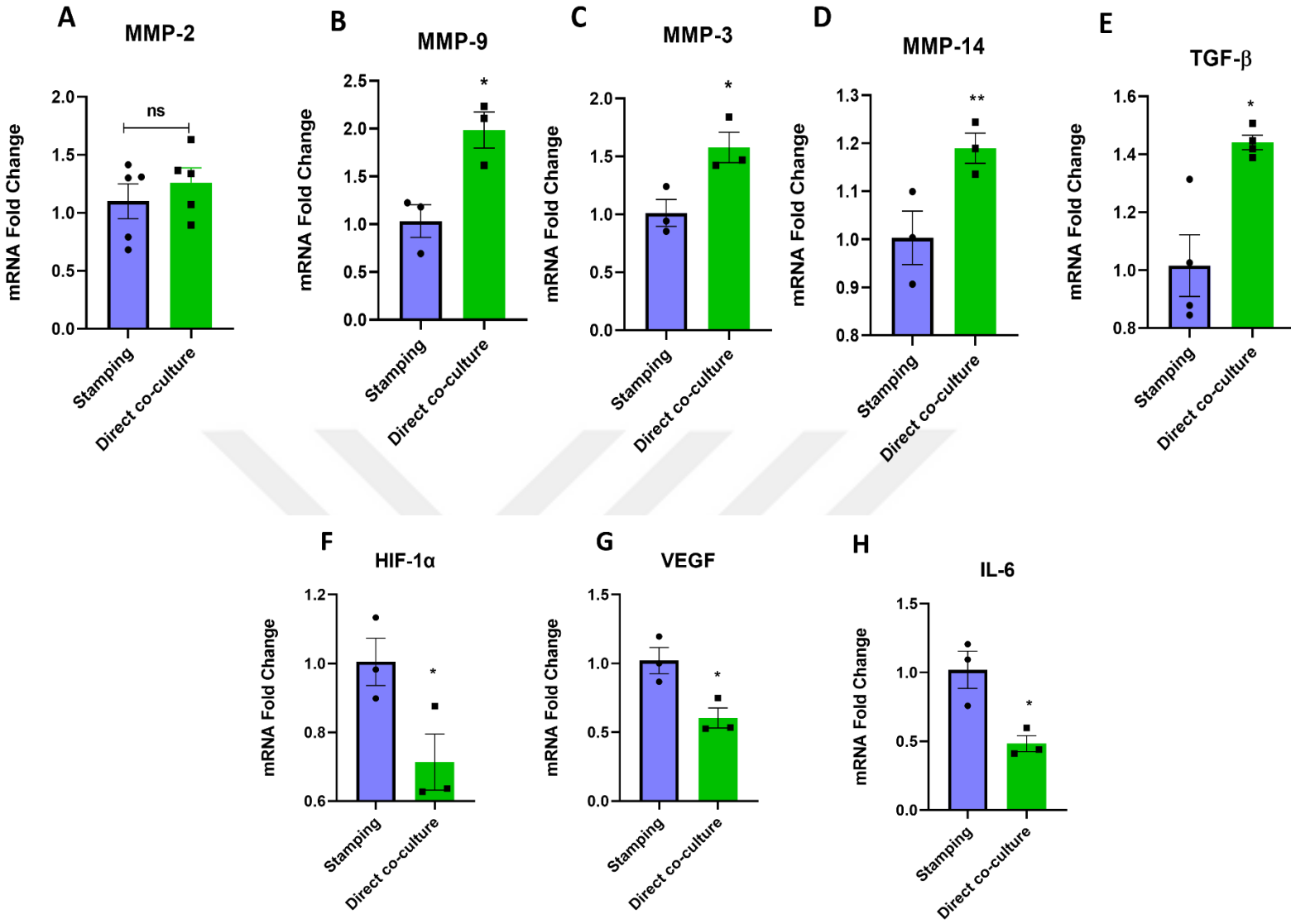

Figure 4.17 The bar charts depict the effect of co-culture configuration type on the gene expression level of the co-culture system. *RNA expression levels were calculated for RNA lysates extracted from gel constructs at Day 7 after encapsulation. Results were calculated with respect to the expression of the housekeeping gene, beta actin, and normalized to the gene expression of cells grown in the "stamping" co-culture configuration. (A-E) Genes demonstrate an elevated expression in the direct co-culture configuration, contrasting with an enhanced expression of genes(F- H) observed in the stamping co-culture setup. The bar charts represent the Mean±SEM of expression values derived from n ≥3 independent experiments, each conducted in triplicate. Statistical significance was assessed using unpaired t-test, denoting (*) for $p < 0.05$, (**) for $p < 0.01$, and (***) $p < 0.001$*

5

CONCLUSIONS AND FUTURE PERSPECTIVES

In conclusion, this thesis focused on the development of a micropatterned 3D hydrogel model of the glioblastoma TME. We microfabricated the astrocyte-glioma 3D co-culture system via a two-step photolithography enabling the precise localization of I-NHA and U87 GBM cell lines in two different co-culture configurations. We further validated the platform by investigating the GBM migration and invasion inside our biomimetic model. This study suggests that the localization of astrocytes within the 3D GelMA platform impacts the GBM migration. While encapsulating I-NHA in close proximity to U87 cells resulted in extensive invasion of the surrounding GelMA matrix; patterning astrocytes around GBM microsperes inhibited tumor migration and sequestered GBM cells by establishing physical barriers in the form of interconnected networks. The interconnected astrocyte networks in the presence of U87 cells unpregulated the GFAP expression, suggesting the reactive transformation of astrocytes and the formation of the glial scar around U87 GBM microspheres. In addition, culturing U87 cells in a 3D environment of GelMA microspheres brought about upregulation of gene expressions related to GBM migration and malignancy. This finding shows the importance of providing cells with a biomimetic environment mimicking the brain ECM properties. The proposed system has the potential to serve as a biomimetic in vitro model for developing clinical strategies targeting GBM migration and TME.

There are several research directions that can be followed in order to shed more light on the effect of astrocyte co-culture and 3D environment on GBM invasiveness and malignancy.

- Although this thesis findings suggest that the astrocyte co-culture configuration type affects the GBM migration, the role of astrocyte direct co-culture on GBM migration remains unclear. The enhanced migration of GBM cells cultured in close proximity

to astrocytes could be the effect of the higher overall density of cells in that configuration. U87 cells in a more crowded environment could favor migration due to available space restrictions. Providing an experimental setup for investigating the role of directly co-cultured astrocytes on GBM migration is a challenging task, but with a careful design it can still be analyzed. So two different setups can be designed: one treating the system as whole, and therefore keeping the overall cell concentration constant, the other varying the astrocyte number, but keeping the U87 cell number constant. To track and quantify the migration, time-lapse microscopy for 12 hours can be used, and individual cell migration can be quantified for parameters such as migration distance, directionality and speed. If both conditions confirm the positive correlation between the astrocyte co-culture and U87 migration, then it can be stated that astrocytes enhance the GBM migration inside our platform.

- The next potential research direction of high importance would be testing anti-cancer drugs on our platform. It would be interesting to investigate the impact of the surrounding astrocyte network on the penetration and efficacy of chemotherapy drugs such as TMZ. Furthermore, the role of astrocytes in GBM treatment resistance inside our platform can also be investigated.

- In our study, while the co-culture of astrocytes with U87 glioblastoma cells did not significantly alter the expression of the genes we specifically investigated, it is plausible that other genes could be affected by this interaction, which remained undetected in our analysis. To delve deeper into the intricate dynamics of cellular interactions inside our micropatterned platform, RNA sequencing could be performed. This technique would enable a comprehensive view of the transcriptomic profile changes in cells co-cultured within our platform, shedding light on how different co-culture configurations influence cellular behavior at the molecular level. Furthermore, to dissect the specific contributions of each cell type in the co-culture, isolating and sorting individual cell populations from the hydrogel matrix is essential. FACS presents a viable method for this separation. Though the process of isolation and sorting may introduce stress to the cells, potentially affecting gene expression and reducing RNA yield, currently, it stands as the most effective

approach for such detailed analysis. This step is crucial for pinpointing the exact cellular interactions and gene expression changes induced by co-culture conditions.

- Although in this thesis, the proposed platform was utilized for mimicking the GBM TME and its interactions with astrocytes, its utility can be greatly enhanced by incorporating a diverse array of cell types beyond astrocytes, including microglia, immune cells, endothelial cells, and oligodendrocytes. In addition, this versatile system can be adapted to model other cancer types where the microenvironment plays a critical role in cancer progression. For example, the platform can be adapted to study the interactions between breast cancer cells and surrounding stromal cells, such as fibroblasts. Furthermore, the platform can also be utilized to investigate the immune evasion mechanisms developed by colorectal cancer by incorporating immune cells into the system. This adaptability opens up new avenues for exploring complex disease mechanisms and testing therapeutic strategies across various cancer types and other diseases where the TME plays a pivotal role.

BIBLIOGRAPHY

Abbas, Z. N., Al-Saffar, A. Z., Jasim, S. M., & Sulaiman, G. M. (2023). Comparative analysis between 2D and 3D colorectal cancer culture models for insights into cellular morphological and transcriptomic variations. *Scientific reports*, *13*(1), 18380.

Adams, K. L., & Gallo, V. (2018). The diversity and disparity of the glial scar. *Nature neuroscience*, *21*(1), 9-15.

Aisenbrey, E. A., & Murphy, W. L. (2020). Synthetic alternatives to Matrigel. *Nature Reviews Materials*, *5*(7), 539-551.

Andersen, B. M., Faust Akl, C., Wheeler, M. A., Chiocca, E. A., Reardon, D. A., & Quintana, F. J. (2021). Glial and myeloid heterogeneity in the brain tumour microenvironment. *Nature Reviews Cancer*, *21*(12), 786-802.

Azam, Z., TO, S. S. T., & Tannous, B. A. (2020). Mesenchymal transformation: the rosetta stone of glioblastoma pathogenesis and therapy resistance. *Advanced Science*, *7*(22), 2002015.

Azevedo Martins, J. M., Rabelo-Santos, S. H., do Amaral Westin, M. C., & Zeferino, L. C. (2020). Tumoral and stromal expression of MMP-2, MMP-9, MMP-14, TIMP-1, TIMP-2, and VEGF-A in cervical cancer patient survival: a competing risk analysis. *BMC cancer*, *20*(1), 1-11.

Beeghly, G. F., Amofa, K. Y., Fischbach, C., & Kumar, S. (2022). Regulation of Tumor Invasion by the Physical Microenvironment: Lessons from Breast and Brain Cancer. *Annual Review of Biomedical Engineering*, *24*(1), 29-59. https://doi.org/10.1146/annurev-bioeng-110220-115419

Biasoli, D., Sobrinho, M., Da Fonseca, A., De Matos, D., Romão, L., de Moraes Maciel, R., Rehen, S., Moura-Neto, V., Borges, H., & Lima, F. (2014). Glioblastoma cells inhibit astrocytic p53-expression favoring cancer malignancy. *Oncogenesis*, *3*(10), e123-e123.

Bikfalvi, A., da Costa, C. A., Avril, T., Barnier, J.-V., Bauchet, L., Brisson, L., Cartron, P. F., Castel, H., Chevet, E., & Chneiweiss, H. (2023). Challenges in glioblastoma research: focus on the tumor microenvironment. *Trends in cancer*, *9*(1), 9-27.

Bouchalova, P., & Bouchal, P. (2022). Current methods for studying metastatic potential of tumor cells. *Cancer Cell International*, *22*(1), 394.

Brandao, M., Simon, T., Critchley, G., & Giamas, G. (2019). Astrocytes, the rising stars of the glioblastoma microenvironment. *Glia*, *67*(5), 779-790.

Brandebura, A. N., Paumier, A., Onur, T. S., & Allen, N. J. (2023). Astrocyte contribution to dysfunction, risk and progression in neurodegenerative disorders. *Nature Reviews Neuroscience*, *24*(1), 23-39.

Brat, D. J., Castellano-Sanchez, A. A., Hunter, S. B., Pecot, M., Cohen, C., Hammond, E. H., Devi, S. N., Kaur, B., & Van Meir, E. G. (2004). Pseudopalisades in Glioblastoma Are Hypoxic, Express Extracellular Matrix Proteases, and Are Formed by an Actively Migrating Cell Population. *Cancer Research*, *64*(3), 920-927. https://doi.org/10.1158/0008-5472.can-03-2073

Bupphathong, S., Quiroz, C., Huang, W., Chung, P.-F., Tao, H.-Y., & Lin, C.-H. (2022). Gelatin methacrylate hydrogel for tissue engineering applications—a review on material modifications. *Pharmaceuticals*, *15*(2), 171.

Caliari, S. R., & Burdick, J. A. (2016). A practical guide to hydrogels for cell culture. *Nature methods*, *13*(5), 405-414.

Campbell, S. C., Muñoz-Ballester, C., Chaunsali, L., Mills III, W. A., Yang, J. H., Sontheimer, H., & Robel, S. (2020). Potassium and glutamate transport is impaired in scar-forming tumor-associated astrocytes. *Neurochemistry international*, *133*, 104628.

CHACON, E., ACOSTA, D., & LEMASTERS, J. J. (1997). Primary cultures of cardiac myocytes as in vitro models for pharmacological and toxicological assessments. *In vitro methods in pharmaceutical research*, 209-223.

Chekhonin, I. V., Chistiakov, D. A., Grinenko, N. F., & Gurina, O. I. (2018). Glioma Cell and Astrocyte Co-cultures As a Model to Study Tumor–Tissue Interactions: A Review of Methods. *Cellular and molecular neurobiology*, *38*(6), 1179-1195.

Chen, C.-W., Yang, C.-H., Lin, Y.-H., Hou, Y.-C., Cheng, T.-J., Chang, S.-T., Huang, Y.-H., Chung, S.-T., Chio, C.-C., & Shan, Y.-S. (2021). The fibronectin expression determines the distinct progressions of malignant gliomas via transforming growth factor-beta pathway. *International Journal of Molecular Sciences*, *22*(7), 3782.

Chen, N., Alieva, M., van der Most, T., Klazen, J. A., Vollmann-Zwerenz, A., Hau, P., & Vrisekoop, N. (2022). Neutrophils Promote Glioblastoma Tumor Cell Migration after Biopsy. *Cells*, *11*(14), 2196.

Chen, R., Smith-Cohn, M., Cohen, A. L., & Colman, H. (2017). Glioma subclassifications and their clinical significance. *Neurotherapeutics*, *14*, 284-297.

Chen, W., Xia, T., Wang, D., Huang, B., Zhao, P., Wang, J., Qu, X., & Li, X. (2016). Human astrocytes secrete IL-6 to promote glioma migration and invasion through upregulation of cytomembrane MMP14. *Oncotarget*, *7*(38), 62425.

Ciasca, G., Sassun, T. E., Minelli, E., Antonelli, M., Papi, M., Santoro, A., Giangaspero, F., Delfini, R., & De Spirito, M. (2016). Nano-mechanical signature of brain tumours. *Nanoscale*, *8*(47), 19629-19643.

Cieśluk, M., Pogoda, K., Piktel, E., Wnorowska, U., Deptuła, P., & Bucki, R. (2022). Mechanical Properties of the Extracellular Environment of Human Brain Cells Drive the Effectiveness of Drugs in Fighting Central Nervous System Cancers. *Brain Sciences*, *12*(7), 927.

Civita, P., M. Leite, D., & Pilkington, G. J. (2019). Pre-clinical drug testing in 2D and 3D human in vitro models of glioblastoma incorporating non-neoplastic astrocytes: tunneling nano tubules and mitochondrial transfer modulates cell behavior and therapeutic response. *International Journal of Molecular Sciences*, *20*(23), 6017.

Cui, Y., Lee, P., Reardon, J. J., Wang, A., Lynch, S., Otero, J. J., Sizemore, G., & Winter, J. O. (2023). Evaluating glioblastoma tumour sphere growth and migration in interaction with astrocytes using 3D collagen-hyaluronic acid hydrogels. *Journal of Materials Chemistry B*.

Daneman, R., & Prat, A. (2015). The blood–brain barrier. *Cold Spring Harbor perspectives in biology*, *7*(1), a020412.

Davis, M. E. (2016). Glioblastoma: overview of disease and treatment. *Clinical journal of oncology nursing*, *20*(5), S2.

Debnath, P., Huirem, R. S., Dutta, P., & Palchaudhuri, S. (2022). Epithelial–mesenchymal transition and its transcription factors. *Bioscience reports*, *42*(1), BSR20211754.

Diep, Y. N., Park, H. J., Kwon, J.-H., Tran, M., Ko, H. Y., Jo, H., Kim, J., Chung, J.-I., Kim, T. Y., & Kim, D. (2023). Astrocytic scar restricting glioblastoma via glutamate–MAO-B activity in glioblastoma-microglia assembloid. *Biomaterials Research*, *27*(1), 71.

Ellert-Miklaszewska, A., Poleszak, K., Pasierbinska, M., & Kaminska, B. (2020). Integrin signaling in glioma pathogenesis: from biology to therapy. *International Journal of Molecular Sciences*, *21*(3), 888.

Etienne-Manneville, S. (2004). Actin and microtubules in cell motility: which one is in control? *Traffic*, *5*(7), 470-477.

Fife, C. M., McCarroll, J. A., & Kavallaris, M. (2014). Movers and shakers: cell cytoskeleton in cancer metastasis. *British journal of pharmacology*, *171*(24), 5507-5523.

Filosa, J. A., Morrison, H. W., Iddings, J. A., Du, W., & Kim, K. J. (2016). Beyond neurovascular coupling, role of astrocytes in the regulation of vascular tone. *Neuroscience*, *323*, 96-109.

Fossati, G., Matteoli, M., & Menna, E. (2020). Astrocytic factors controlling synaptogenesis: a team play. *Cells*, *9*(10), 2173.

Gagliano, N., Costa, F., Cossetti, C., Pettinari, L., Bassi, R., Chiriva-Internati, M., Cobos, E., Gioia, M., & Pluchino, S. (2009). Glioma-astrocyte interaction modifies the astrocyte phenotype in a co-culture experimental model. *Oncology reports*, *22*(6), 1349-1356.

Gauthier, L. R., Saati, M., Bensalah-Pigeon, H., Ben M'Barek, K., Gitton-Quent, O., Bertrand, R., Busso, D., Mouthon, M.-A., Collura, A., & Junier, M.-P. (2020). The HIF1α/JMY pathway promotes glioblastoma stem-like cell invasiveness after irradiation. *Scientific reports*, *10*(1), 18742.

Guan, X., Hasan, M. N., Maniar, S., Jia, W., & Sun, D. (2018). Reactive astrocytes in glioblastoma multiforme. *Molecular Neurobiology*, *55*, 6927-6938.

Gupta, R. K., Niklasson, M., Bergström, T., Segerman, A., Betsholtz, C., & Westermark, B. (2024). Tumor-specific migration routes of xenotransplanted human glioblastoma cells in mouse brain. *Scientific reports*, *14*(1), 864.

Habanjar, O., Diab-Assaf, M., Caldefie-Chezet, F., & Delort, L. (2021). 3D cell culture systems: tumor application, advantages, and disadvantages. *International Journal of Molecular Sciences*, *22*(22), 12200.

Haim, L., Carrillo-de Sauvage, M., Ceyzériat, K., & Escartin, C. (2015). Elusive roles for reactive astrocytes in neurodegenerative diseases. Front Cell Neurosci 9: 278. In.

Hashimoto, N., Kitai, R., Fujita, S., Yamauchi, T., Isozaki, M., & Kikuta, K.-I. (2023). Single-Cell Analysis of Unidirectional Migration of Glioblastoma Cells Using a Fiber-Based Scaffold. *ACS Applied Bio Materials*, *6*(2), 765-773.

He, J., Sun, Y., Gao, Q., He, C., Yao, K., Wang, T., Xie, M., Yu, K., Nie, J., & Chen, Y. (2023). Gelatin Methacryloyl Hydrogel, from Standardization, Performance, to Biomedical Application. *Advanced Healthcare Materials*, 2300395.

Henrik Heiland, D., Ravi, V. M., Behringer, S. P., Frenking, J. H., Wurm, J., Joseph, K., Garrelfs, N. W., Strähle, J., Heynckes, S., & Grauvogel, J. (2019). Tumor-associated reactive astrocytes aid the evolution of immunosuppressive environment in glioblastoma. *Nature communications*, *10*(1), 2541.

Herrera-Perez, R. M., Voytik-Harbin, S. L., Sarkaria, J. N., Pollok, K. E., Fishel, M. L., & Rickus, J. L. (2018). Presence of stromal cells in a bioengineered tumor microenvironment alters glioblastoma migration and response to STAT3 inhibition. *PLoS One*, *13*(3), e0194183.

Hidalgo, M., & Eckhardt, S. G. (2001). Development of matrix metalloproteinase inhibitors in cancer therapy. *Journal of the National Cancer Institute*, *93*(3), 178-193.

Xu, H., Casillas, J., Krishnamoorthy, S., & Xu, C. (2020). Effects of Irgacure 2959 and lithium phenyl-2, 4, 6-trimethylbenzoylphosphinate on cell viability, physical properties, and microstructure in 3D bioprinting of vascular-like constructs. *Biomedical Materials*, *15*(5), 055021.

Imamura, Y., Mukohara, T., Shimono, Y., Funakoshi, Y., Chayahara, N., Toyoda, M., Kiyota, N., Takao, S., Kono, S., & Nakatsura, T. (2015). Comparison of 2D-and 3D-culture models as drug-testing platforms in breast cancer. *Oncology reports*, *33*(4), 1837-1843.

Inoue, A., Ohnishi, T., Nishikawa, M., Ohtsuka, Y., Kusakabe, K., Yano, H., Tanaka, J., & Kunieda, T. (2023). A Narrative Review on CD44's Role in Glioblastoma Invasion, Proliferation, and Tumor Recurrence. *Cancers*, *15*(19), 4898.

Johnson, D. E., O'Keefe, R. A., & Grandis, J. R. (2018). Targeting the IL-6/JAK/STAT3 signalling axis in cancer. *Nature reviews Clinical oncology*, *15*(4), 234-248.

Joseph, J. V., Conroy, S., Tomar, T., Eggens-Meijer, E., Bhat, K., Copray, S., Walenkamp, A. M., Boddeke, E., Balasubramanyian, V., & Wagemakers, M. (2014). TGF-β is an inducer of ZEB1-dependent mesenchymal transdifferentiation in glioblastoma that is associated with tumor invasion. *Cell death & disease*, *5*(10), e1443-e1443.

Kasten, B. B., Jiang, K., Cole, D., Jani, A., Udayakumar, N., Gillespie, G. Y., Lu, G., Dai, T., Rosenthal, E. L., & Markert, J. M. (2020). Targeting MMP-14 for dual PET and fluorescence imaging of glioma in preclinical models. *European journal of nuclear medicine and molecular imaging*, *47*, 1412-1426.

Kaur, B., Khwaja, F. W., Severson, E. A., Matheny, S. L., Brat, D. J., & Van Meir, E. G. (2005). Hypoxia and the hypoxia-inducible-factor pathway in glioma growth and angiogenesis. *Neuro-oncology*, *7*(2), 134-153.

Khademhosseini, A., & Langer, R. (2007). Microengineered hydrogels for tissue engineering. *Biomaterials*, *28*(34), 5087-5092.

Khoonkari, M., Liang, D., Kamperman, M., Kruyt, F. A., & van Rijn, P. (2022). Physics of brain cancer: Multiscale alterations of glioblastoma cells under extracellular matrix stiffening. *Pharmaceutics*, *14*(5), 1031.

Kieseier, B. C., Seifert, T., Giovannoni, G., & Hartung, H.-P. (1999). Matrix metalloproteinases in inflammatory demyelination: targets for treatment. *Neurology*, *53*(1), 20-20.

Kim, Y., & Kumar, S. (2014). CD44-mediated adhesion to hyaluronic acid contributes to mechanosensing and invasive motility. *Molecular Cancer Research*, *12*(10), 1416-1429.

Klotz, B. J., Gawlitta, D., Rosenberg, A. J., Malda, J., & Melchels, F. P. (2016). Gelatin-methacryloyl hydrogels: towards biofabrication-based tissue repair. *Trends in biotechnology*, *34*(5), 394-407.

Krawczynski, K., Godlewski, J., & Bronisz, A. (2020). Oxidative stress—Part of the solution or part of the problem in the hypoxic environment of a brain tumor. *Antioxidants*, *9*(8), 747.

Qiang, L., Wu, T., Zhang, H., Lu, N., Hu, R., Wang, Y., Zhao, L., Chen, F., Wang, X., & You, Q. (2012). HIF-1α is critical for hypoxia-mediated maintenance of glioblastoma stem cells by activating Notch signaling pathway. *Cell Death & Differentiation*, *19*(2), 284-294.

Quintero-Fabián, S., Arreola, R., Becerril-Villanueva, E., Torres-Romero, J. C., Arana-Argáez, V., Lara-Riegos, J., Ramírez-Camacho, M. A., & Alvarez-Sánchez, M. E. (2019). Role of matrix metalloproteinases in angiogenesis and cancer. *Frontiers in oncology*, *9*, 1370.

Le, D. M., Besson, A., Fogg, D. K., Choi, K.-S., Waisman, D. M., Goodyer, C. G., Rewcastle, B., & Yong, V. W. (2003). Exploitation of astrocytes by glioma cells to facilitate invasiveness: a mechanism involving matrix metalloproteinase-2 and the urokinase-type plasminogen activator–plasmin cascade. *Journal of Neuroscience*, *23*(10), 4034-4043.

Lee, E.-J., Kim, S.-Y., Hyun, J.-W., Min, S.-W., Kim, D.-H., & Kim, H.-S. (2010). Glycitein inhibits glioma cell invasion through down-regulation of MMP-3 and MMP-9 gene expression. *Chemico-biological interactions*, *185*(1), 18-24.

Li, R., Li, G., Deng, L., Liu, Q., Dai, J., Shen, J., & Zhang, J. (2010). IL-6 augments the invasiveness of U87MG human glioblastoma multiforme cells via up-regulation of MMP-2 and fascin-1. *Oncology reports*, *23*(6), 1553-1559.

Lo Dico, A., Martelli, C., Diceglie, C., Lucignani, G., & Ottobrini, L. (2018). Hypoxia-inducible factor-1α activity as a switch for glioblastoma responsiveness to temozolomide. *Frontiers in oncology*, *8*, 249.

Loeffler, S., Fayard, B., Weis, J., & Weissenberger, J. (2005). Interleukin-6 induces transcriptional activation of vascular endothelial growth factor (VEGF) in astrocytes in vivo and regulates VEGF promoter activity in glioblastoma cells via direct interaction between STAT3 and Sp1. *International journal of cancer*, *115*(2), 202-213.

Loessner, D., Meinert, C., Kaemmerer, E., Martine, L. C., Yue, K., Levett, P. A., Klein, T. J., Melchels, F. P., Khademhosseini, A., & Hutmacher, D. W. (2016). Functionalization, preparation and use of cell-laden gelatin methacryloyl–based hydrogels as modular tissue culture platforms. *Nature Protocols*, *11*(4), 727-746.

Mahajan, S. D., Law, W.-C., Aalinkeel, R., Reynolds, J., Nair, B. B., Yong, K.-T., Roy, I., Prasad, P. N., & Schwartz, S. A. (2012). Nanoparticle-mediated targeted delivery of antiretrovirals to the brain. In *Methods in Enzymology* (Vol. 509, pp. 41-60). Elsevier.

Mair, D. B., Ames, H. M., & Li, R. (2018). Mechanisms of invasion and motility of high-grade gliomas in the brain. *Molecular Biology of the Cell*, *29*(21), 2509-2515. https://doi.org/10.1091/mbc.e18-02-0123

Malric, L., Monferran, S., Gilhodes, J., Boyrie, S., Dahan, P., Skuli, N., Sesen, J., Filleron, T., Kowalski-Chauvel, A., & Moyal, E. C.-J. (2017). Interest of integrins targeting in glioblastoma according to tumor heterogeneity and cancer stem cell paradigm: An update. *Oncotarget*, *8*(49), 86947.

Marhuenda, E., Fabre, C., Zhang, C., Martin-Fernandez, M., Iskratsch, T., Saleh, A., Bauchet, L., Cambedouzou, J., Hugnot, J.-P., & Duffau, H. (2021). Glioma stem cells invasive phenotype at optimal stiffness is driven by MGAT5 dependent

mechanosensing. *Journal of experimental & clinical cancer research*, *40*(1), 1-14.

Mohiuddin, E., & Wakimoto, H. (2021). Extracellular matrix in glioblastoma: Opportunities for emerging therapeutic approaches. *American Journal of Cancer Research*, *11*(8), 3742.

Monteiro, A. R., Hill, R., Pilkington, G. J., & Madureira, P. A. (2017). The role of hypoxia in glioblastoma invasion. *Cells*, *6*(4), 45.

Nakod, P. S., Kim, Y., & Rao, S. S. (2021). The impact of astrocytes and endothelial cells on glioblastoma stemness marker expression in multicellular spheroids. *Cellular and Molecular Bioengineering*, *14*, 639-651.

Nemeth, C. L., Janebodin, K., Yuan, A. E., Dennis, J. E., Reyes, M., & Kim, D.-H. (2014). Enhanced chondrogenic differentiation of dental pulp stem cells using nanopatterned PEG-GelMA-HA hydrogels. *Tissue Engineering Part A*, *20*(21-22), 2817-2829.

Ngo, M. T., & Harley, B. A. (2019). Perivascular signals alter global gene expression profile of glioblastoma and response to temozolomide in a gelatin hydrogel. *Biomaterials*, *198*, 122-134.

Nguyen, A. K., Goering, P. L., Reipa, V., & Narayan, R. J. (2019). Toxicity and photosensitizing assessment of gelatin methacryloyl-based hydrogels photoinitiated with lithium phenyl-2, 4, 6-trimethylbenzoylphosphinate in human primary renal proximal tubule epithelial cells. *Biointerphases*, *14*(2).

Nieland, L., Morsett, L. M., Broekman, M. L., Breakefield, X. O., & Abels, E. R. (2021). Extracellular vesicle-mediated bilateral communication between glioblastoma and astrocytes. *Trends in Neurosciences*, *44*(3), 215-226.

Oishi, T., Koizumi, S., & Kurozumi, K. (2022). Molecular Mechanisms and Clinical Challenges of Glioma Invasion. *Brain Sciences*, *12*(2), 291. https://doi.org/10.3390/brainsci12020291

Peela, N., Sam, F. S., Christenson, W., Truong, D., Watson, A. W., Mouneimne, G., Ros, R., & Nikkhah, M. (2016). A three dimensional micropatterned tumor model for breast cancer cell migration studies. *Biomaterials*, *81*, 72-83.

Pullen, N. A., Pickford, A. R., Perry, M. M., Jaworski, D. M., Loveson, K. F., Arthur, D. J., Holliday, J. R., Van Meter, T. E., Peckham, R., & Younas, W. (2018). Current insights into matrix metalloproteinases and glioma progression: Transcending the degradation boundary. *Metalloproteinases In Medicine*, 13-30.

Rabah, N., Ait Mohand, F.-E., & Kravchenko-Balasha, N. (2023). Understanding Glioblastoma Signaling, Heterogeneity, Invasiveness, and Drug Delivery Barriers. *International Journal of Molecular Sciences*, *24*(18), 14256. https://doi.org/10.3390/ijms241814256

Rath, B. H., Fair, J. M., Jamal, M., Camphausen, K., & Tofilon, P. J. (2013). Astrocytes enhance the invasion potential of glioblastoma stem-like cells. *PLoS One*, *8*(1), e54752.

Rauti, R., Renous, N., & Maoz, B. M. (2020). Mimicking the brain extracellular matrix in vitro: a review of current methodologies and challenges. *Israel Journal of Chemistry*, *60*(12), 1141-1151.

Saraswathibhatla, A., Indana, D., & Chaudhuri, O. (2023). Cell–extracellular matrix mechanotransduction in 3D. *Nature Reviews Molecular Cell Biology*, 1-22.

Schmitz, C., Pepelanova, I., Ude, C., & Lavrentieva, A. (2022). Studies on oxygen availability and the creation of natural and artificial oxygen gradients in gelatin-

methacryloyl hydrogel 3D cell culture. *Journal of Tissue Engineering and Regenerative Medicine*, *16*(11), 977-986.

Seker-Polat, F., Pinarbasi Degirmenci, N., Solaroglu, I., & Bagci-Onder, T. (2022). Tumor cell infiltration into the brain in glioblastoma: from mechanisms to clinical perspectives. *Cancers*, *14*(2), 443.

Senft, C., Priester, M., Polacin, M., Schröder, K., Seifert, V., Kögel, D., & Weissenberger, J. (2011). Inhibition of the JAK-2/STAT3 signaling pathway impedes the migratory and invasive potential of human glioblastoma cells. *Journal of neuro-oncology*, *101*, 393-403.

Shah, N., Hallur, P. M., Ganesh, R. A., Sonpatki, P., Naik, D., Chandrachari, K. P., Puchalski, R. B., & Chaubey, A. (2021). Gelatin methacrylate hydrogels culture model for glioblastoma cells enriches for mesenchymal-like state and models interactions with immune cells. *Scientific reports*, *11*(1), 17727.

Sharma, P., Aaroe, A., Liang, J., & Puduvalli, V. K. (2023). Tumor microenvironment in glioblastoma: Current and emerging concepts. *Neuro-Oncology Advances*, *5*(1), vdad009.

Shieh, L.-T., Guo, H.-R., Chang, Y.-K., Lu, N.-M., & Ho, S.-Y. (2020). Clinical implications of multiple glioblastomas: An analysis of prognostic factors and survival to distinguish from their single counterparts. *Journal of the Formosan Medical Association*, *119*(3), 728-734.

Shirahama, H., Lee, B. H., Tan, L. P., & Cho, N.-J. (2016). Precise tuning of facile one-pot gelatin methacryloyl (GelMA) synthesis. *Scientific reports*, *6*(1), 31036.

Sofroniew, M. V., & Vinters, H. V. (2010). Astrocytes: biology and pathology. *Acta neuropathologica*, *119*, 7-35.

Sohrabi, A., Lefebvre, A. E., Harrison, M. J., Condro, M. C., Sanazzaro, T. M., Safarians, G., Solomon, I., Bastola, S., Kordbacheh, S., & Toh, N. (2023). Microenvironmental stiffness induces metabolic reprogramming in glioblastoma. *Cell Reports*, *42*(10).

Sternlicht, M. D., & Werb, Z. (2001). How matrix metalloproteinases regulate cell behavior. *Annual review of cell and developmental biology*, *17*(1), 463-516.

Sun, P., Mu, Y., & Zhang, S. (2014). A novel NF-κB/MMP-3 signal pathway involves in the aggressivity of glioma promoted by Bmi-1. *Tumor Biology*, *35*, 12721-12727.

Sun, Z., Guo, S. S., & Fässler, R. (2016). Integrin-mediated mechanotransduction. *Journal of Cell Biology*, *215*(4), 445-456.

Takahashi, Y., Hori, Y., Yamamoto, T., Urashima, T., Ohara, Y., & Tanaka, H. (2015). 3D spheroid cultures improve the metabolic gene expression profiles of HepaRG cells. *Bioscience reports*, *35*(3), e00208.

Tamai, S., Ichinose, T., Tsutsui, T., Tanaka, S., Garaeva, F., Sabit, H., & Nakada, M. (2022). Tumor microenvironment in glioma invasion. *Brain Sciences*, *12*(4), 505.

Tekin, H., Simmons, S., Cummings, B., Gao, L., Adiconis, X., Hession, C. C., Ghoshal, A., Dionne, D., Choudhury, S. R., & Yesilyurt, V. (2018). Effects of 3D culturing conditions on the transcriptomic profile of stem-cell-derived neurons. *Nature biomedical engineering*, *2*(7), 540-554.

Tian, X., Azpurua, J., Hine, C., Vaidya, A., Myakishev-Rempel, M., Ablaeva, J., Mao, Z., Nevo, E., Gorbunova, V., & Seluanov, A. (2013). High-molecular-mass hyaluronan mediates the cancer resistance of the naked mole rat. *Nature*, *499*(7458), 346-349.

Ulasov, I., Yi, R., Guo, D., Sarvaiya, P., & Cobbs, C. (2014). The emerging role of MMP14 in brain tumorigenesis and future therapeutics. *Biochimica et Biophysica Acta (BBA)-Reviews on Cancer*, *1846*(1), 113-120.

Valkonen, M., Haapasalo, H., Rilla, K., Tyynelä-Korhonen, K., Soini, Y., & Pasonen-Seppänen, S. (2018). Elevated expression of hyaluronan synthase 2 associates with decreased survival in diffusely infiltrating astrocytomas. *BMC cancer*, *18*, 1-11.

Vasile, F., Dossi, E., & Rouach, N. (2017). Human astrocytes: structure and functions in the healthy brain. *Brain Structure and Function*, *222*(5), 2017-2029.

Verhaak, R. G. W., Hoadley, K. A., Purdom, E., Wang, V., Qi, Y., Wilkerson, M. D., Miller, C. R., Ding, L., Golub, T., Mesirov, J. P., Alexe, G., Lawrence, M., O'Kelly, M., Tamayo, P., Weir, B. A., Gabriel, S., Winckler, W., Gupta, S., Jakkula, L., Feiler, H. S., Hodgson, J. G., James, C. D., Sarkaria, J. N., Brennan, C., Kahn, A., Spellman, P. T., Wilson, R. K., Speed, T. P., Gray, J. W., Meyerson, M., Getz, G., Perou, C. M., & Hayes, D. N. (2010). Integrated Genomic Analysis Identifies Clinically Relevant Subtypes of Glioblastoma Characterized by Abnormalities in PDGFRA, IDH1, EGFR, and NF1. *Cancer Cell*, *17*(1), 98-110. https://doi.org/10.1016/j.ccr.2009.12.020

Vollmann-Zwerenz, A., Leidgens, V., Feliciello, G., Klein, C. A., & Hau, P. (2020). Tumor Cell Invasion in Glioblastoma. *International Journal of Molecular Sciences*, *21*(6), 1932. https://doi.org/10.3390/ijms21061932

Wang, C., Sinha, S., Jiang, X., Murphy, L., Fitch, S., Wilson, C., Grant, G., & Yang, F. (2021). Matrix stiffness modulates patient-derived glioblastoma cell fates in three-dimensional hydrogels. *Tissue Engineering Part A*, *27*(5-6), 390-401.

Wang, L., Zuo, X., Xie, K., & Wei, D. (2018). The role of CD44 and cancer stem cells. *Cancer Stem Cells: Methods and Protocols*, 31-42.

Wang, M., Wang, T., Liu, S., Yoshida, D., & Teramoto, A. (2003). The expression of matrix metalloproteinase-2 and-9 in human gliomas of different pathological grades. *Brain tumor pathology*, *20*, 65-72.

Weller, M., Wick, W., Aldape, K., Brada, M., Berger, M., Pfister, S. M., Nishikawa, R., Rosenthal, M., Wen, P. Y., & Stupp, R. (2015). Glioma. *Nature reviews Disease primers*, *1*(1), 1-18.

West, A. J., Tsui, V., Stylli, S. S., Nguyen, H., Morokoff, A. P., Kaye, A. H., & Luwor, R. B. (2018). The role of interleukin-6-STAT3 signalling in glioblastoma. *Oncology letters*, *16*(4), 4095-4104.

Wolf, K. J., Chen, J., Coombes, J. D., Aghi, M. K., & Kumar, S. (2019). Dissecting and rebuilding the glioblastoma microenvironment with engineered materials. *Nature Reviews Materials*, *4*(10), 651-668.

Wu, W., Klockow, J. L., Zhang, M., Lafortune, F., Chang, E., Jin, L., Wu, Y., & Daldrup-Link, H. E. (2021). Glioblastoma multiforme (GBM): An overview of current therapies and mechanisms of resistance. *Pharmacological Research*, *171*, 105780.

Yang, J., Antin, P., Berx, G., Blanpain, C., Brabletz, T., Bronner, M., Campbell, K., Cano, A., Casanova, J., & Christofori, G. (2020). Guidelines and definitions for research on epithelial–mesenchymal transition. *Nature Reviews Molecular Cell Biology*, *21*(6), 341-352.

Yue, K., Trujillo-de Santiago, G., Alvarez, M. M., Tamayol, A., Annabi, N., & Khademhosseini, A. (2015). Synthesis, properties, and biomedical applications of gelatin methacryloyl (GelMA) hydrogels. *Biomaterials*, *73*, 254-271.

Zhang, C.-b., Wang, Z.-l., Liu, H.-j., Wang, Z., & Jia, W. (2023). Characterization of tumor-associated reactive astrocytes in gliomas by single-cell and bulk tumor sequencing. *Frontiers in Neurology*, *14*, 1193844.
Zhang, H., Zhou, Y., Cui, B., Liu, Z., & Shen, H. (2020). Novel insights into astrocyte-mediated signaling of proliferation, invasion and tumor immune microenvironment in glioblastoma. *Biomedicine & Pharmacotherapy*, *126*, 110086.
Zhong, J., Paul, A., Kellie, S. J., & O'Neill, G. M. (2010). Mesenchymal migration as a therapeutic target in glioblastoma. *Journal of oncology*, *2010*.
Zhou, W., Yu, X., Sun, S., Zhang, X., Yang, W., Zhang, J., Zhang, X., & Jiang, Z. (2019). Increased expression of MMP-2 and MMP-9 indicates poor prognosis in glioma recurrence. *Biomedicine & Pharmacotherapy*, *118*, 109369.

APPENDIX

1. MATLAB code for image processing

```
direct1_astrocytes_day7_masked = imread("/MATLAB Drive/Astrocytes/direct1-astrocytes_day7_masked.tif");
direct1_Astrocytes_day5 = imread("/MATLAB Drive/Astrocytes/direct1-Astrocytes_day5.tif");
direct1_Astrocytes_day3 = imread("/MATLAB Drive/Astrocytes/direct1_Astrocytes_day3.tif");



imshow(direct1_Astrocytes_day3)imshow(direct1_Astrocytes_day3)
title("Astrocytes direct day 3")


# converting images into grayscale

grayAstD3=im2gray(direct1_Astrocytes_day3);
imshow(grayAstD3)
title("Astrocytes Day 3 in gray scale")



adjAstD3=imadjust(grayAstD3)

imhist(adjAstD3)
```

```
  title("Adjusted Histogram")
imhist(adjAstD3)


#adding a circle onto an image that covers the region of the doughnut


  adjAstD3Circle = insertShape(adjAstD3,"filledcircle",[150 280 35],LineWidth=5);

  imshow(adjAstD3Circle)
  adjAstD3Circle = insertShape(adjAstD3,"filledcircle",[512 512 35],LineWidth=5);
imshow(adjAstD3Circle)

 gray_direct1_Ast=im2gray(direct1_Astrocytes)
 adj_gray_direct1_Ast=imadjust(gray_direct1_Ast)
 circle_adj_gray_direct1_Ast = insertShape(adj_gray_direct1_Ast,"filledcircle",[150
 280 35],LineWidth=5)
 circle_adj_gray_direct1_Ast = insertShape(adj_gray_direct1_Ast,"filledcircle",[530
 550 400],LineWidth=5)

 masked_adj_gray_direct1_Ast = insertShape(adj_gray_direct1_Ast,'filledcircle',[530
 550 400],'LineWidth',5 , 'color',[1 1 1])

 N=numel(circle_adj_gray_direct1_Ast)


 props = regionprops("table",BW,"all")

 props = regionprops("table",BW,"all")

 sum(props.Area)


 bw_adj_gray_direct1_Ast = createBinaryMask(adj_gray_direct1_Ast

 >> AreaPixels= sum(props_bw_adj_gray_circle_Stamping1_U87_1D5.Area)
% Adjust data to span data range.
X = imadjust(X);

% Threshold image with manual threshold
BW = im2gray(X) > 75;

% Open mask with square
width = 4;
se = strel('square', width);
BW = imopen(BW, se);

% Create masked image.
```

```
maskedImage = X;
maskedImage(~BW) = 0;
end
```

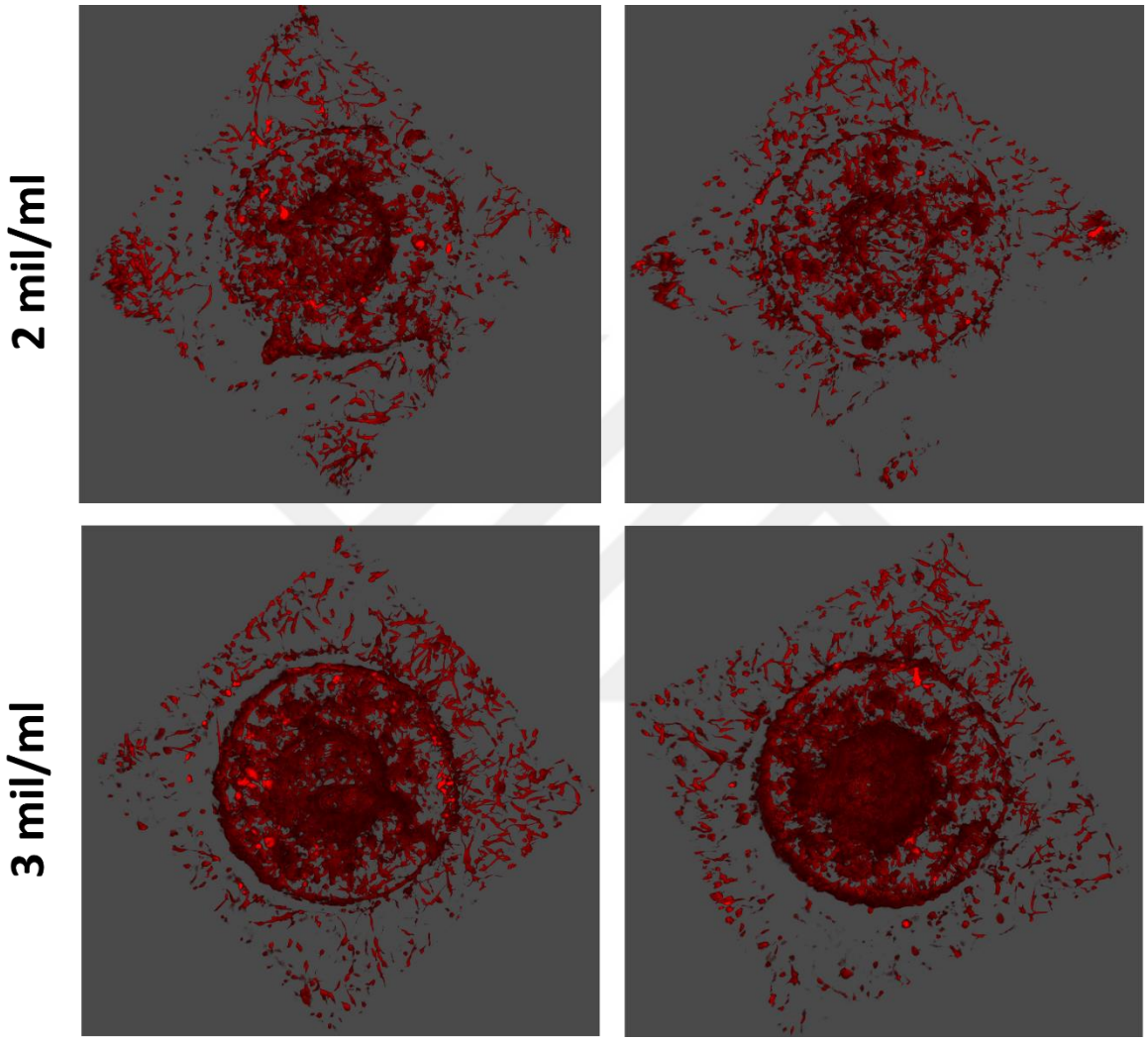

Figure A.1 The 3D projections of representative images comparing the migration and cell density of 3mil/ml and 2mi/ml U87 cells encapsulated within GelMA doughnuts. *Images were taken with confocal microscope at Day 7 of culture. Scalebar represents 200µm.*

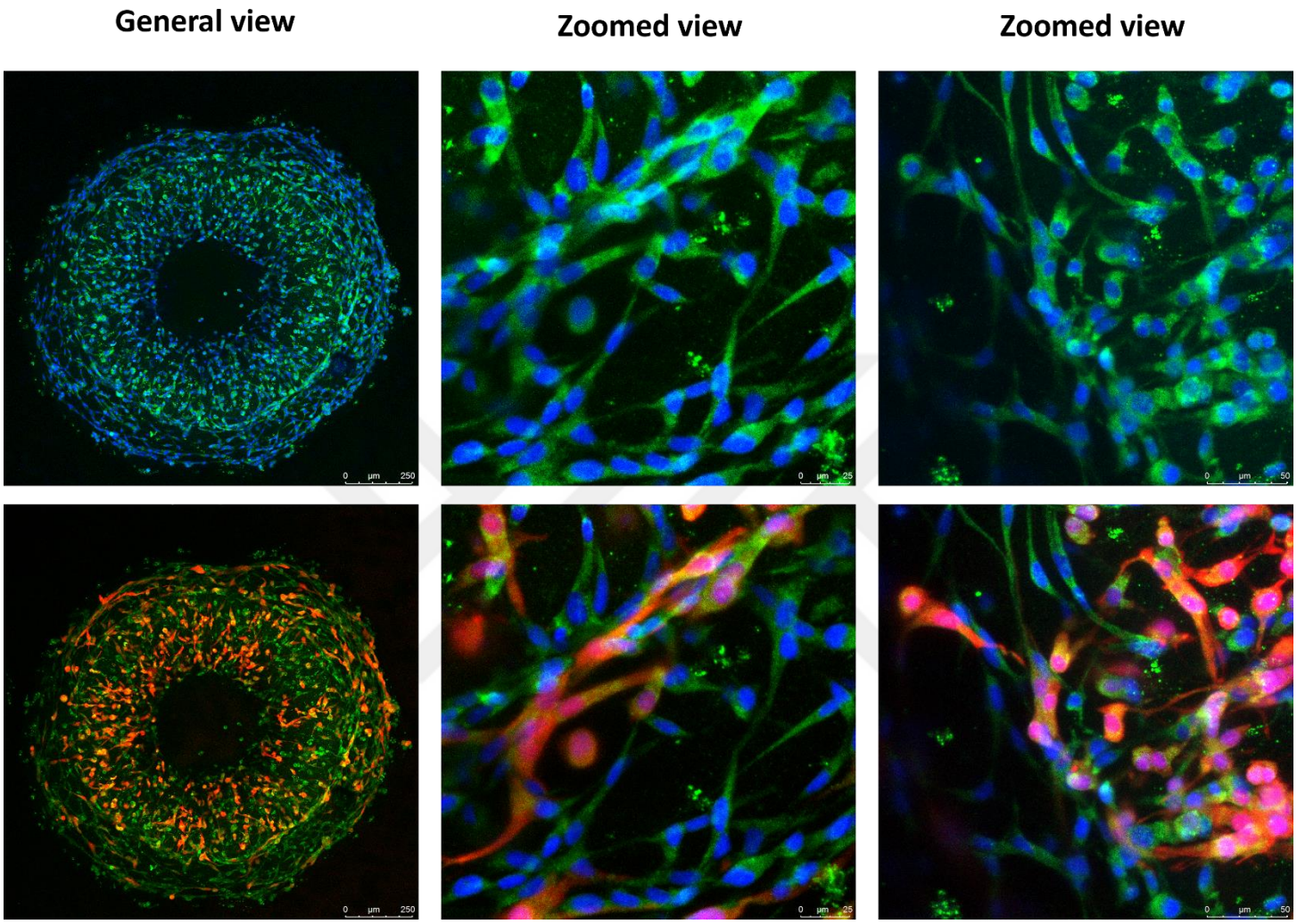

Figure A.2 Immunocytochemical staining against MMP-2 in co-cultured I-NHA with U87. *U87 cells are tagged with RFP, while I-NHA are not. Both cell types express high levels of MMP-2, exhibiting high biodegradability of GelMA hydrogel constructs. The zoomed images demonstrate the formation of connections between RFP-tagged U87(red) and MMP-2 stained I-NHA (green). Scalebar for the general view is 250μm, and 25 μm and 50 μm for zoomed images, respectively.*